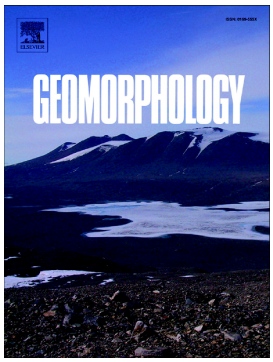

Near surface geophysical analysis of the Navamuño depression (Sierra de Béjar, Iberian Central System): Geometry, sedimentary infill and genetic implications of tectonic and glacial footprint

Rosa M. Carrasco, Valentí Turu, Javier Pedraza, Alfonso Muñoz-Martín, Xavier Ros, Jesús Sánchez, Blanca Ruiz-Zapata, Antonio J. Olaiz, Ramón Herrero-Simón

PII: S0169-555X(18)30181-8
DOI: doi:10.1016/j.geomorph.2018.05.003
Reference: GEOMOR 6390

To appear in: *Geomorphology*

Received date: 27 January 2017
Revised date: 16 April 2018
Accepted date: 1 May 2018

Please cite this article as: Rosa M. Carrasco, Valentí Turu, Javier Pedraza, Alfonso Muñoz-Martín, Xavier Ros, Jesús Sánchez, Blanca Ruiz-Zapata, Antonio J. Olaiz, Ramón Herrero-Simón , Near surface geophysical analysis of the Navamuño depression (Sierra de Béjar, Iberian Central System): Geometry, sedimentary infill and genetic implications of tectonic and glacial footprint. The address for the corresponding author was captured as affiliation for all authors. Please check if appropriate. Geomor(2017), doi:10.1016/j.geomorph.2018.05.003

Near surface geophysical analysis of the Navamuño depression (Sierra de Béjar, Iberian Central System): Geometry, sedimentary infill and genetic implications of tectonic and glacial footprint

Rosa M. Carrasco[a], Valentí Turu[b], Javier Pedraza[c], Alfonso Muñoz-Martín[c,g], Xavier Ros[b], Jesús Sánchez[a], Blanca Ruiz-Zapata[d], Antonio J. Olaiz[e], Ramón Herrero-Simón[f],

[a] Dpt. of Geological and Mining Engineering, Univ. of Castilla-La Mancha, Avda. Carlos III, s/n, 45071 Toledo, Spain.

[b] Fundacio Marcel Chevallier, Edifici Socio-Cultural de La LLacuna, AD500 Andorra la Vella, Principality of Andorra.

[c] Dpt. of Geodynamic, Complutense University, C/ José Antonio Novais, 12, 28040 Madrid, Spain.

[d] Dpt. of Geology, Alcalá University, Ctra. A-II km 33,600, 28871 Alcalá de Henares, Madrid.

[e] Non Seismic Methods. Repsol Exploration, c/ Méndez Álvaro, 44, 28045, Madrid, Spain.

[f] Dpt. de Física i Enginyeria Nuclear, Polytechnic University of Catalonia (UPC). Física Ed. TR1 (EET) C/Colom, 1, 08222 Terrassa.

[g] Instituto de Geociencias – IGEO (UCM, CSIC), C/ José Antonio Novais, 12, 28040 Madrid, Spain.

*Corresponding author. Tel.: +34 925268800

E-mail address: Rosa.Carrasco@uclm.es (R.M. Carrasco)

Abstract

The geometric and genetic characterization of the Navamuño depression peatland system (Iberian Central System) is presented here using results from a geophysical survey. This depression is a ~30 ha pseudo-endorheic flat basin over granitic bedrock. Three geophysical techniques were used to map the subsurface geology, and identify and describe the infill sequence: shallow seismic refraction (SR), magnetic resonance sounding (MRS) and electrical resistivity measurements (VES and ERT). The three main geoelectrical layers (G1, G2, G3) identified in previous research, have also been identified in the present work. Using the data obtained in this new research we have been able to analyse these three geological layers in detail and reinterpret them. They can be grouped genetically into two sedimentary units: an ancient sedimentary body (G3), of unknown age and type, beneath an Upper Pleistocene (G2) and Holocene (G1) sedimentary infill. The facies distribution and geometry of the Upper Pleistocene was examined using the Sequence Stratigraphy method, revealing that the Navamuño depression was an ice-dammed in the last glacial cycle resulting in glaciolacustrine sedimentation. A highly permeable sedimentary layer or regolith exists beneath the glaciolacustrine deposits. Below 40 m depth, water content falls dramatically down to a depth of 80 m where unweathered bedrock may be present. The information obtained from geophysical, geological and geomorphological studies carried out in this research, enabled us to consider various hypotheses as to the origin of this depression. According to these data, the Navamuño depression may be explained as the result of a transtensional process from the Puerto de Navamuño strike-slip fault during the reactivation of the Iberian Central System (Paleogene-Lower Miocene, Alpine orogeny), and can be correlated with the pull-apart type basins described in these areas. The neotectonic activity of this fault and the ice-dammed processes in these areas during the Last Glacial Cycle (MIS2) were the main causes of recent sedimentary infill in this depression.

Keywords: Near Surface Geophysics, Nuclear Magnetic Resonance, intermontain basin, distensive faulting, Late Glacial Period, Iberian Central System.

1. Introduction

The small endorheic depressions known as *navas* are flat, treeless areas, usually intermontain and sometimes marshy, common throughout the Iberian Central System (ICS). The recent sedimentary evolution of these depressions involves slope, fluvial and nival processes, and in some cases glacial and fluvioglacial processes (Pedraza, 1994). As a result, these depressions have traditionally been studied to reconstruct the environmental conditions pertaining in the ICS during the Quaternary (see Ruiz-Zapata et al., 2011; López-Sáez et al., 2014). However, only very limited data have been obtained to date relating to our understanding of the glacial record in these areas (Ruiz-Zapata et al., 2011; López-Sáez et al., 2016). In previous studies, the sedimentary infill analysed was of limited thickness (3 - 6 m), mainly homogeneous (often only two sedimentary sequences appear) and not pre-Holocene in age (e.g. Franco-Múgica, 1995; Rubiales et al., 2007; López-Sáez et al., 2014; Abel-Schaad et al., 2014; Génova et al., 2016).

Taking these precedents into account, one of the aims of the research which commenced several years ago into the ICS Pleistocene glaciation (Carrasco et al., 2009) was to carry out a geological and geophysical prospective of these *nava*-type depressions located in the former glacial areas. In the Navamuño depression (ND), one of the navas analysed, a series of indicators was detected enabling the working hypothesis that the ND is a unique case in the ICS. This interpretation was based on the thickness of the sediments hosted by the depression and their posible genetic relationship with the neotectonic activity and glacial dynamics of the Cuerpo de

Hombre, one of the reference paleoglaciers used for glacier evolution research in the ICS (Carrasco et al., 2015a, 2015b).

With this approach, the main aim of this study is to establish in detail the geometry of the ND, and interpret the thickness and sequence of its sedimentary infill and its genetic context. Previous works (Ruiz-Zapata et al., 2011; Carrasco et al., 2015a, 2015b; Turu et al., 2018) provided the essential data to support the present study of the ND trough.

The methods chosen with this aim in mind were based on those applied in other mountain systems in the Iberian Peninsula using geophysical techniques supported by detailed geological surveys (Vilaplana and Casas, 1983; Bordonau, 1992; Turu 1999; Turu et al., 2007, 2011; Pélachs et al., 2011; Pellicer et al., 2012; Salazar-Rincón et al., 2013). Taking as a base the three resistivity levels identified in a previous study (G1, G2, G3; Carrasco et al., 2015a), Electrical Resistivity Tomography (ERT), Vertical Electrical Sounding (VES), Magnetic Resonance Sounding (MRS) and Seismic Refraction (SR) have been applied in the ND for detecting and defining the presence of sharp geological contacts (ERT and SR) such as faults or buried paleo-relief, sub-horizontal stratigraphy (VES) and aquifers (MRS).

2. Geological and geomorphological setting

2.1. Regional context

The ND is located at 1500 m above sea level (asl) on the western versant of the Sierra de Béjar (ICS, Fig. 1) with a surface area of ~30.76 ha. This depression is confined between scarped slopes on the granitic basement and one of the moraines of the Cuerpo de Hombre paleoglacier (Fig. 2). The bottom of the depression is a seasonal flood-plain with peatland development, currently dissected by fluvial channels.

ND forms part of the fracture corridor associated with the Puerto de Navamuño fault (PN fault) and has been classified as a Variscan strike-slip fault (Bellido-Mulas, 2006) associated with the NE-trending strike-slip faults of Alentejo-Plasencia (AP; a.k.a. Plasencia, Odemira-Plasencia, or Messejana-Plasencia; > 500 km) and Hervás-Candelario (HC; around 40 km) (Fig. 1). Together these faults are responsible for the Jerte-Aravalle and Hervás-Candelario corridor-type valleys which limit the Sierra de Béjar pop-up (Sanz-Donaire, 1979; Moreno, 1991; Carrasco, 1997).

All these reliefs were formed during the Alpine Orogeny as the result of the transmission to the interior of the Iberian Plate of the compressive stress generated at its edges due to collision with Eurasia during the lower Oligocene-Miocene (Cantabrian-Pyrenean) and with Africa since 9 Ma (De Vicente and Vegas, 2009). De Vicente et al. (2007) and De Vicente (2009) propose partitioning of deformation in the ICS with a generalized NNW-SSE shortening in a transpressive regime. This regime has not varied substantially from the Oligocene to the present, although its maximum intensity was concentrated during the Lower Eocene-Miocene (Continental Iberia-Eurasia collision). Fission track dating (De Bruijne and Andriessen, 2002), seismic (Olaiz et al., 2009; Muñoz-Martín et al., 2012), and GPS (Garate et al., 2015) data confirm this model.

Minor depressions such as the ND are common throughout the ICS and the Iberian Massif and have been analysed in depth along the AP fault (Brum da Silveira, 1990; Carrasco and Pedraza, 1991; Cabral, 1995, 2012; Capote et al., 1996; Brum da Silveira et al., 2009; De Vicente et al., 2011; Villamor et al., 2012). According to these data, these depressions originated in the Paleogene-Lower Miocene as pull-apart type sedimentary basins and some of them continued active throughout the Miocene. Others, however, halted at the start of the Upper Miocene and their function changed to shallow sedimentary basins regulated by neotectonic readjustments during the recents times (Upper Pliocene and Quaternary). In other ICS depressions developed on a rock substratum (El Burguillo and Alto Tormes valleys; Fig. 1), some anomalies detected in

the layout of the current drainage network have also been interpreted as indicators of neotectonic activity (Vazquez et al., 1987; Pol et al., 1989).

Although this area of the ND is presently characterized by moderate to very low seismic activity, according to instrumental and historical records (IGN, 2016), the 1755 Lisbon earthquake (Mendes-Victor et al., 2009) originated small-scale slope movements in the Valle del Jerte (11.83 km SE of ND) and resulted in cracks in the walls and partial roof collapse in some monumental buildings in the city of Plasencia (40.53 km SW of ND) (Carrasco, 1997; Udías and López-Arroyo, 2009). On the other hand, and this is one of the fundamental points under debate, the neotectonic activity of these faults during the Quaternary is framed within the context of low deformation rates, reflected in the presence of slow faults with much longer return periods than the time period covered by the historical or instrumented seismic data (Cabral, 2012; Foroutan et al., 2016).

The lithological context of the ND substratum is that of the Sierra de Béjar, which forms part of one of the most important granitic batholiths of the Iberian Massif (Villaseca et al., 1999; Villaseca, 2003). The most abundant rocks in the area are monzogranites and Variscan granodiorites, with associated migmatites, schists, quartzites and other pre-Variscan metasediments. In the ICS, and the Iberian Massif in general, various supergenic weathering sequences have been identified in these granitic substrata. The oldest (pre-Tertiary), thick weathering mantles correspond to laterite profiles (Molina-Ballesteros et al., 1991, 1997). The most recent weathering mantles (Tertiary and in some cases Quaternary) are less thick, sometimes sub-surficial, and are associated with wash-exposure rock weathering stages and therefore their transformation levels vary, ranging from simple bisialitization (predominance of montmorillonite) to monosialitization (predominance of kaolinite) (Centeno and Brell, 1987; Molina-Ballesteros et al., 1994).

2.2. Study area and hypothesis

In earlier studies of the ND (Carrasco et al., 2015a), a sedimentary trough was detected, occupying part of the depression and hosting sediments calculated to be approx. 60 m thick. The sedimentary sequence, established from lithological data (16 m test bore) and from data obtained using geophysics, consists of three geoelectrical layers (Carrasco et al., 2015a; Turu et al., 2018): G1 (10-18 m thick), nearest the surface, interpreted as coarse sand with intercalated clays and silts, sometimes presenting zones with organic material indicating the presence of paleochannels and/or peatbog zones; G2 (7-10 m thick in some zones, 40-50 m thick in others), interpreted either as a sedimentary debris-flow deposit, highly porous, coarse-grained, and saturated with water (arkosic), or as arenized granite; and G3 substratum of the trough on non-weathered granitic rock. The nomenclature of these layers has been maintained in this research, although the layers may be redefined with the new data obtained. ^{14}C dating establishes approximate ages of 5700 BP for a sample located at 485 cm and 10000 BP at a level one meter lower (565-570 cm) and 13720 BP for a level located at depth 16 m (Ruiz-Zapata et al., 2011; Carrasco et al., 2015a; Turu et al., 2018).

These earlier studies mentioned the possibility that the evolution of the sedimentary trough in ND was related to an obstruction process generated by the left-lateral moraine of the Cuerpo de Hombre paleoglacier, which defines the eastern margin of the depression. The abrupt change of direction presented by this left lateral moraine of the Cuerpo de Hombre, aligned along NW-SE and NNE-SSW structures, has also been highlighted in various studies (Rubio, 1990; Carrasco et al., 2013, 2015b). This left-lateral moraine forms part of the morphostratigraphic formation called ‘principal moraine’ (PM), and has been used as reference to establish the evolutive sequence of the ICS paleoglaciers (Pedraza, 2012; Pedraza et al., 2013; Carrasco et al., 2013).

The evolutive sequence in the Cuerpo de Hombre paleoglacier was dated using ^{10}Be-TCN technique on scattered erratic blocks or moraine boulders. As a result of this work, the following ages have been established (Carrasco et al., 2015b) (Fig. 2A, 2C): (1) glacial maximum (~25.0 ka; MIS2); (2) some retreat and stabilization stages formed after ~24.3 ka and before ~20.6 ka; (3) some readvance and stabilization phases shown by the PM formation, dated later than ~20.6 ka and earlier than ~17.8 ka; and (4) a deglaciation process showing three stadials in the late glacial sequence dated to (minimum ages) ~17.5 ka, ~13.9 ka and ~11.1 ka.

All these earlier data as well as those corresponding to the regional geological context described in the previous section, were used as the basis for the central hypothesis on which the new research described herein was planned and carried out. This hypothesis considers that the primary origin of the ND converged with the pull-apart type basins described in these areas, and its recent evolution was associated with some tectonic readjustments and with the Cuerpo de Hombre paleoglacier. Thus, the chronoevolutive sequence of this paleoglacier has been used as reference to establish the sequence and chronology of the infill stages of the ND depression during the obstruction period.

This is a topic of general interest in the study of paleoglaciers, since it related to the impact of non-climatic factors on glacier dynamics and therefore on the typology and arrangement of geomorphological indicators used as reference to establish chronologies, evolutive sequences and global paleoclimatic deductions (Olvmo and Johansson, 2002; Ber, 2009; Glasser and Ghiglione, 2009; Cotton et al., 2014; Yanites and Ehlers, 2012; Prasicek et al., 2015; Bathrellos et al., 2017).

3. Methods

3.1. Surficial geology and fracture network

Geological mapping was produced using vertical aerial photographs (Scale 1: 10000 and 1:18000) and PNOA-2014 orthophotos (Instituto Geográfico Nacional, IGN). This procedure and field surveys were used to define the geological and geomorphological units presented in this study.

There was abundant information previously available on the bedrock lithology (Bellido-Mulas, 2006) and the glacial morphology of the Sierra de Béjar and its immediate surroundings as a whole, including the ND (Sanz-Donaire, 1979; Rubio 1990; Carrasco, 1997; Carrasco et al., 2013, 2015a, 2015b). Nevertheless, the boundaries of the depression and contacts between the different lithological formations have had to be mapped with new, complementary data. A detailed morphotectonic information has also been produced which includes scarps, alignments, fractures and fracture corridors. The main aim of this information is to contribute a complementary data series to the geophysical research into the deposits hosted in the depression, as this is where the search has been focused for indicators to interpret the genesis and evolution of this depression and the possible existence of neotectonic activity. This methodological approach takes into account the precedents described above in Section 2.0 to interpret neotectonic activity in these areas. In all cases, indicators of this activity have been obtained in the sedimentary fill in the depressions (fractured or folded sediments, abrupt or anomalous contacts, etc.). This is because the data provided by the rock substrate formations are limited to some faceted surfaces and anomalies in the drainage network which are often difficult to interpret and must be obtained by studying wider areas than the intermontain depressions. On the other hand, this information is a basis for correlation with morphostructures established at a regional level in other depressions similar to the ND, such as the Amblés, Jerte and Garganta del Villar valleys (Fig. 1).

The aim of the field work was to carry out a detailed review of the geological formations obtained from photointerpretation and to characterize the typology of some surficial formations not analysed in previous studies. In this review special attention

was paid to the location and typology of weathered bedrock materials (*grus*), as in some cases these formations present hydrogeological, geotechnical and geophysical characteristics similar to the arkose formations which appear in some ICS intermontain depressions.

3.2. Geophysical methods

3.2.1. Vertical electrical soundings (VES) and Electrical resistivity tomography (ERT)

Electrical resistivity methods (VES and ERT) consist of obtaining the apparent resistivity (ρ_{ap}) of rocks and soils from the voltages observed in potential electrodes, in response to the introduced DC intensity in the current electrodes. If the distance between the current electrodes is gradually increased in relation to a central point, the vertical resistivity distribution can be examined, i.e. in 1D (VES). In ERT an electrode array is deployed laterally along a profile, obtaining a 2D resistivity model of a subsoil section (Reynolds, 2011). The ERT results obtained enable an understanding of the bedrock geometry and differentiate infill types from their contrasting electrical resistivity (Descloitres et al., 2008; Hausmann et al., 2013).

VES data acquisition was completed in 3 survey campaigns: the first two provided a preliminary estimation of the depression geometry (Carrasco et al., 2015a) and the third completed the data required to define the geometry and produce the final infill model. All VES were carried out with a Schlumberger-type configuration and the maximum array length is 266 m (Fig. 3). For a correct interpretation, the 'apparent' resistivity values (i.e. the mean value of the rock volume affected by the current flow) must be converted to 'real' resistivity of the different subsoil units using an inversion process, in either 1D (VES, Zohdy, 1989; Barker, 1992) or 2D (ERT, Loke and Barker, 1996; Loke et al., 2010). In the case of VES, due to the principle of electrical equivalence (Maillet, 1947; Bhattacharya and Patra, 1968; Reynolds, 2011), there is

inherent uncertainty in the method, in that the electrical behaviour of a layer is defined by the combination of its thickness and its resistivity, which may generate important uncertainty. This uncertainty is limited or resolved by: (1) an equivalence analysis and (2) inclusion of other subsoil survey techniques. In the ND the VES inversion and equivalence analysis were performed using Moscow State University IPI2Win free software (Bobachev et al., 2003), obtaining a 1D resistivity model and corresponding equivalence analysis (see supplementary material).

ERT data were collected in field work using a RESECS DMT 64 channel resistivity meter with 5 m spacing between electrodes. Nine profiles were measured with lengths from 205 - 275 m (Fig. 3). Wenner and Dipole-Dipole electrode configurations were used and the maximum depth reached was 70 m.

RES2DINV software (Loke and Barker, 1996; Loke et al., 2010) was used for field data inversion. A normal inversion algorithm using 4-node finite element modelling has been used. The size of the elements was the same as the distance between electrodes (5 m). The resistivity data were of very good quality with high S/N ratio, and repeat measurement errors below 1%. The ND data inversion models gave consistently low error statistics with RMS <3%. The result of all this information, combined with VES, enabled a better understanding of the 2D distribution of the different geo-resistive bodies and how they relate to surface geomorphological and geological data.

3.2.2. Magnetic resonance sounding (MRS)

The MRS technique is applied in different geological contexts (Behroozmand et al., 2015), and allows quantification of porosity, permeability and thickness of aquifer levels to a depth of the first 150 m (Yaramanci, 2000; Vouillamoz et al., 2007; Lange et al., 2007; Mejías and Plata, 2007; Plata and Rubio, 2008; Hertrich, 2008).

MRS is based on the properties of nuclear magnetic resonance (NMR) which uses the resonance produced in protons subjected to a magnetic field with a specific frequency. The method consists in energising the terrain with an increasing electromagnetic pulse moment (q, in A·ms) generated in a loop, with the aim of penetrating deeper into the subsoil (Table 1). When the pulse terminates, the terrain response is logged as initial amplitude, (E_0 in nV), decay time (ms) and phase (degrees). The initial amplitude value (E_0) is directly related to the amount of water contained in the soil to the slice depth affected by the pulse, while the decay time (T2*) depends on the hydraulic permeability. To suppress random noise and improve the signal/noise ratio, each pulse is repeated several times for signal-stacking purposes. Greater depth is reached in the research by increasing the value of q, with a maximum depending on the loop dimensions. The test sounding consists of various measurements of increasing values of q, to establish functions E_0 and T2* as a function of q.

These parameters depend on the electrical conductivity of the subsoil, magnetic field (inclination and magnitude), loop size, electromagnetic noise and possible presence of magnetic rocks (Weichman et al., 2000; Hertrich, 2008).

Two MRS soundings were carried out in the ND at the same point but using different sized loop (30x30 m and 60x60 m) (Fig. 3). This survey method has been successfully tested in other geological contexts (Turu, 2012; Behroozmand et al., 2015) with a twofold aim: to achieve sounding to the maximum depth possible with the apparatus used but without resolution loss in the first tens of meters of the subsoil. NMR data were collected in the field using Iris-Instruments NUMIS LITE equipment which can penetrate to maximum depth 90 m. The field data inversion was performed using Shushakov and Legchenko (1994) and Legchenko and Shushakov (1998) methods, and the results obtained enabled 1D quantification of the hydrogeological parameters mentioned above.

3.2.3. Seismic refraction (RS)

Seismic techniques are often used to study Quaternary deposits and research the subsoil layers, paleorelief geometry and geomechanical properties of surficial deposits (Turu, 1999; Turu et al., 2007; Schrott et al., 2003; Yamakawa et al., 2012). This technique is based on measuring the travel time of P waves which travel directly or critically refracted to a geophone array deployed along a seismic line (Sheriff and Geldart, 1991; Reynolds, 2011). Analysis of the travel times picks from each source to the geophone array are plotted as time/distance curves on a time-distance graph. The qualitative analysis of these travel times using the general reciprocal method (GRM) (Palmer, 1980), or tomographic techniques (Watanabe et al., 1999; Sheehan et al., 2005), enables reconstruction of the contacts between different media (refractors) and the depth distribution of the P wave velocities. The seismic source used varies depending on the test depth, and a sledge hammer is usually used in superficial studies to reach depths of up to 25 m.

The results obtained by seismic refraction are a 2D vertical section of the P wave velocity distribution (V_P), with lateral resolution defined by the distance between the geophones (normally 1 - 5 m).

The seismic survey in the ND centred on the axial zone and on its northern margins. Five 48 m-long seismic refraction profiles were generated, with geophones regularly spaced at 6 m intervals (Fig. 3). The seismic waves were generated by percussion with a 6 kg hammer on a metal plate placed on the ground, with shooting points at each end and in the centre of the profile. As the ND is included in a Special Protection Area for birds, more efficient seismic wave generation methods were ruled out.

The seismograph used was a 16-channel prototype designed by the Universidad Politécnica de Cataluña (UPC). Signal processing and inversion was performed using specific software (Anasim 6.0; Herrero-Simón, 2003) which allows

detection of refracted and reflected waves and subsequent subsoil characterization using models of inclined layers (velocity, depth and inclination). This was particularly useful in the peat bog profiles, as the low ground compaction muffled the signal generated with the hammer. The results obtained were verified using Simusism2 software (Herrero-Simón, 2007), also produced by the UPC, which simulates seismic wave propagation in subsoils with random velocity distribution.

The aim of the seismic refraction was to define the contact between low-velocity to higher-velocity layers, such as from overburden to bedrock and/or highly weathered rocks, and from peat to clastic sediments. Also the presence of discontinuities in the upper surface of the basement, produced by faults and/or erosive surfaces. In these cases, sharp contacts such as occur in a gully or in faults, delay the wave arrival time and disturb the dromochronic representation. Where this occurs, the throw can be calculated as the delay is exponentially related to the seismic velocity of the layers involved.

4. Results and interpretation

Although the ND is generally rectangular in shape, bounded by mainly rectilinear scarped slopes, when analysed in detail the boundaries are found to be more complex. The slopes forming the northen and western sides are formed on granitic rocks (monzogranites and porphyritic biotite granodiorite; Bellido-Mulas, 2006) and associated with NE-SW and NNE-SSW fractures (Fig. 4). The mainly rectilinear northern boundary is due to a minor ENE-WSW fault. The western boundary is less regular, with directional changes originating in a series of minor faults, which displace the two main NNE-SSW and NNW-SSE faults. These morphostructural differences are also clearly seen in the fluvial plain forming the floor of the depression and in the granitic materials. The northern area of this fluvial plain is directly linked to the scarped slope with a clear knickpoint slope break and the granitic rock appears fairly fresh. In

the western part, however, between the scarped slope and the fluvial plain, intermediate minor *glacis* reliefs are seen, formed on the weathered rock substratum *grus* and surficial deposits (lithosoils and slope deposits; Figs. 2B, 5).

The granitic materials are in general unweathered and very heavily fractured. The weathered rock is found in bands associated with fractures, and on the surface forms a regolith composed of grus, scree and soil. In places where the weathered rock can be observed in situ, and in line with standard field classifications (Anon, 1977; Dearman, 1978), two degrees of transformation can be identified: Grade III (moderate), in which the rock shows general discolouration and is easily broken by hand, although the majority of minerals are recognizable most of the original textures have been lost; and Grade II (slight), in which the original minerals, textures and structures of the rock are recognizable (although the rock is difficult to break up by hand and there are abundant fragments of fresh rock) but shows discolouration due to migration of iron oxides resulting from the transformation of certain minerals, particularly biotite.

The southern boundary is more complex and is defined by a system of steps and shoulders due to two fault sets, one parallel to and the other conjugate with the PN fault. These steps have been fossilized and smoothed by the outermost surficial deposits of the Cuerpo de Hombre paleoglacier and by a torrential fan system. All these geomorphical features penetrate into the interior of the depression and mark the southern limit of the base fluvial plain. Finally, the eastern boundary, defined by the slope corresponding to the left lateral moraine of the Cuerpo de Hombre paleoglacier, is fairly rectilinear and is parallel to the western side, with a clearly defined contact with the depression base fluvial plain (Figs. 2, 5).

The base of the depression is a fluvial plain where a channel system forms a general network pattern, with occasional meanders or anastomosis and some flood zones where small peatland and marshy fomations accumulate.

4.1. Vertical Electrical Soundings (VES)

Three geoelectrical layers have been detected in the ND, confirming and complementing previously obtained data (Carrasco et al., 2015a). These layers are called G1, G2 and G3 from highest to lowest (Table 2, Fig. 5).

The first resistive layer (G1) is found immediately under the ground surface and has variable resistivity, due to its heterogeneous lithological composition. In general terms, it is 3-4 m thick, although in the southernmost part of the depression centre, a thickness of up to 20 m has been detected (VES 8).

The second resistive layer (G2) obtains resistivity values ranging from 500 - 800 Ωm, except in the distal zone of the depression (between VES 5 and 9) which exhibits contrasting resistivity values of 250-300 Ωm. Where geoelectrical layer G2 has been identified, the thickness varies, oscillating between 20 and 50 m.

The third resistive layer (G3) corresponds to the deepest sediment levels deposited in the depression and overall this layer displays resistivity values between 600 and 1600 Ωm.

In general, stacking of the three geoelectrical layers is observed but exceptions are found at the edges of the depression. Close to the moraine (Fig. 5) the three geoelectrical levels described are detected in VES 1 position, and also resistive deposits which form the lateral moraine of the Cuerpo de Hombre paleoglacier (Fig. 6, ERT 1 and ERT 2). In contrast, the geoelectrical layers are not present above the moraine sediments (VES 3). The absence of contrasting electric resistivity between levels G3 and G2 in the central sector of the depression (VES 6) makes them difficult to separate with this survey method. In the northern sector (VES 4) the existence of the nearby crystalline basement did not facilitate sedimentation of all the geoelectrical layers. The granitoid basement with characteristic relatively high resistivity (around 2000 Ωm) was identified in the central area of the depression (VES 7 and VES 8) from the abrupt slope change shown by the resistivity curve, otherwise it is difficult to detect,

as for example in VES 4 and 6. VES 5 is the only one with an H-type curve, which means that the second layer has a lower resistivity than the one above and the one below. For this reason, VES 9 was carried out nearby. The final VES has 4 layers and any significant continuity in the intermediate layer is ruled out. For this reason, a dashed line is drawn between VES 9 and VES 5 on the map in Fig. 5.

4.2. Electrical Resistivity Tomography (ERT)

The depth reached in the ERT sections ranged between 40 and 60 m and the three geoelectrical layers defined above (and previously, Carrasco et al., 2015a) are identified, i.e. G1, G2 and G3 (Fig. 6).

Geoelectrical layer G1 exhibits the greatest resistivity (1600 - 16000 Ωm). This implies genetically that G1 has a larger overall grain size and a lower silt and clay content (cf. Waxman and Smits, 1968). In geometric terms, there are notable thickness variations of this layer (ERT 3, Fig. 6). Sedimentary accretion (ERT 3 and ERT 7, Fig. 6) denotes greater accommodation northwards, at the depression centre.

The contact between layer G1 and the other two layers displays paraconformity in ERT 3, and overall concordance in ERT 1 and ERT 7, above all towards the depression centre (ERT 2 and ERT 8, Fig. 6). In G1, the onlap contact of the resistive materials in ERT 7 and ERT 1 is observed with sedimentary aggradation towards the depression centre. Less marked onlap contact can also be deduced from the synsedimentary tilting of the base of layer G2 in the central part of the depression (ERT 2). These onlap contacts are interpreted as tilting (as in ERT 2) or fossilization of fault scarps (as in ERT 7 and ERT 1) which affect the basement rock (layer G3). The subsidence activity would then be responsible for the synsedimentary accretion towards the north in layers G1 and G2 (ERT 1 and ERT 7). Finally, the granitic substratum which forms the depression boundary is identified by the sharp lateral resistivity contrasts with layers G2 and G3 (ERT 2 and ERT 8, Fig. 6). This sharp

contact is interpreted as the confinement of sedimentary infill by sinking of the rock basement. Subsidence activity would then be responsible for the synsedimentary accretion towards the north in layers G1 and G2 (ERT 1 and ERT 7). Finally, the granitic substratum which forms the depression boundary is identified by the sharp lateral resistivity contrasts with layers G2 and G3 (ERT 2 and ERT 8, Fig. 6). This sharp contact indicated in Fig. 6 is interpreted as the confinement of sedimentary infill by sinking of the granite basement.

Geoelectrical layer G2 is more heterogeneous than G1 and with lower resistivity (20 - 2000 Ωm). This layer exhibits greater geometrical development towards the centre of the basin and marked lateral variations in resistivity, especially in the central zone of the depression (ERT 2, ERT 8, Fig. 6). Thus, the fine-grained sedimentary facies (silts and clays) are interpreted in the conductive nuclei in ERT 2 and ERT 8 and should be attributed to lacustrine environment deposits. On the contrary, the most resistive bodies correspond to coarse-grained sedimentary facies (sands and gravels), attributable to fluvial environment deposits (ERT 2, Fig 6).

Geoelectrical layer G3 corresponds to the lower level of the ND infill, with low resistivity (200 - 2000 Ωm) contrasting with the rock substratum resistivity (2000 - 20000 Ωm). This geoelectrical layer rests directly on the resistive rock substratum in the centre of the depression (ERT 2 and ERT 8, Fig. 6). In the southern sector of the depression, G3 presents an important vertical variation in resistivity and also horizontal variation, although to a lesser degree. In e.g. ERT 7, vertical values range from 3 kΩ m to up to ten times lower. In contrast, the horizontal resistivity ratio is half of that detected on the left margin of ERT 1 and ERT 3 and that of the opposite edge (Fig. 6). These resistivity variations can be interpreted as variations in the sedimentary infill grain size, just as in geoelectrical layer G2. However, the nature of the geoelectrical layer G3 is unknown, in contrast to that of G1 and G2 which have been identified by

Carrasco et al. (2015a) in a 8 m-deep borehole performed in the centre of the depression.

Three test bores were performed in ND, with one reaching a maximum depth 16 m, and used for paleoenvironmental studies (Ruiz-Zapata et al., 2011; Carrasco et al., 2015a; Turu et al., 2018). In this sounding, 3 layers can be distinguished from top to bottom: the top layer (0-300 cm) is composed of clayey silt interspersed with gravel (geoelectric unit G1); the second layer (300-800 cm) comprises sands with beds of finely-laminated clay to 500 cm, and then sands and gravels interspersed with beds of clays and silts to the bottom of the sounding (geoelectric unit G2). Carbon-14 dating presented in Carrasco et al. (2015a) and Turu et al. (2018) shows approximate ages of 5700 BP for a sample located at 485 cm and 13720 BP for a level located at depth 16 m. This indicates that in the central part of the depression, the bottomset is Late Glacial in age.

4.3. Magnetic Resonance Sounding (MRS)

Two double pulse MRS were performed in ND. Quantitative results show that contact with the impermeable substratum is located at a depth of approximately 80 m, while at 50 - 70 m there is a zone with gradually decreasing porosity and permeability (Figs. 7C, 7D). Interpretation of the field-curve data from the two surveys undertaken suggests that water is present in all geoelectrical layers in the first 30 m (Fig. 7C), decreasing the water content from 30 to 60 m depth. The main aquifer is found in the first 40 m from the subsurface, although it reflects the inherent heterogeneity of the depression infill sedimentary deposits (Fig. 7C). The infill layer down to 40 m, containing the main aquifer, corresponds to electrical units G1 and G2, while the zone with gradually decreasing permeability (40 - 80 m) corresponds to unit G3. This unit exhibits relatively high values of resistivity with lateral changes, and a progressive decrease in water content and permeability. The most likely interpretation of its nature

are the following: (1) that it is a sedimentary infilling with a lower porosity towards its base; and (2) that it is a zone of altered basement rock, with a maximum alteration at its top, and a reduction with depth.

Water is not detected in the main aquifer at depths of 13 - 17 m. Given that only free water is detected by MRS, this apparently small quantity of water can only be justified by the presence of low porosity in clay deposits. In addition, the free water presence in the clay displays a very short relaxation time (Fig. 7D) in the MRS signal and may not be detected due to instrumental limitations (Turu, 2012). The relaxation time of the water signal is a permeability-related parameter (Mejías and Plata, 2007) and both T2* and T1 show a wide range of values (Figs. 7E, 7F). This is interpreted as significant infill grain-size variability, ranging from clay and silt (100 ms; Fig. 7E) to sand and gravel (values higher than 300 ms; Fig. 7F). However, T2* and T1 relaxation times do not converge at all depths. Usually T1 > T2* but in the case that they are not, T1 measurements are more approximate and pseudo-saturation recovery complications would not produce a 90º pulse and distribution of tip angles, reducing the estimation of T1 (Grunewald and Knight, 2011). This is the case for Fig. 7E at a 22 m depth; here T2* > T1 (Fig. 3F), just at the bottom of the inferred fine grained deposits or low resistive (ERT 8, Fig. 6). If T2* << T1 then paramagnetic geology produces inhomogeneous field dephasing, due to magnetic grains or field-scale magnetic anomalies reducing T2* relaxation time (Walsh, 2008). This seems to be the case below a depth of 36 m, where T2* is systematically lower than T1.

4.3. Seismic Refraction (RS)

The seismic refraction sections performed along the northern edge of the depression allowed the reconstruction of an NW-SE transect to 15-20 m in depth (Fig. 8). In this section the contact can be observed between the sedimentary infill (Vp between 350 and 1350 m/s, Table 3) and the rock substratum (Vp > 1800 m/s). Minor

variations in sedimentary fill velocity were observed, interpreted as erosive surfaces, but in general terms the refractions fit a stratified model.

In profile RS1 delays can be observed in the refracted wave reception time (Fig 8), which is linked to sharp contacts attributable to filled gullies, as those described by Turu et al. (2018). In the sector of this profile near the slope and in RS5, the presence of rock substratum is characterized by high seismic velocity. In profile RS4, beneath the moraine and at a shallow depth, the rock substratum has also been detected from its seismic velocity (ERT 8, Fig. 6 and Table 3). The geological units detected in RS3 and RS4 are different at the edge of the lateral moraine which is the boundary of the ND, interpreted as an onlap contact between the moraine and the depression infill (Fig. 8). The absence of refracted waves in this part of the profile is due to an inversion of the seismic velocity (V1>V2), implying that the underlying deposits are less dense than those nearer the surface. The explanation for this anomaly may be related to the presence of a pressurized aquifer.

A refractor located at a depth of 9 m was identified in the overlap of the two seismic profiles RS3 and RS2 (Fig. 8). Because of its continuity and increasing depth towards the centre of the depression, this layer can be catalogued as a first order reflector equivalent to the division of the sedimentary fill between the geoelectric layers G2 and G3 in the electrical tomography profiles (ERT 8).

4.4. Stratigraphic architecture inferred from geophysical data

The architecture of the infill examined can be subdivided into depositional sequences and system tracts, as has already been carried out in other glacial obstruction depressions (Jalut et al., 2010; Turu et al., 2017). The limits between depositional sequences are the result of stratigraphic discontinuities and their correlative surfaces throughout the basin under analysis (Vail et al., 1987). It is therefore important to identify them from the layer geometry or sharp changes in their

properties (Turu et al., 2017). Based on this, unconformity surfaces (US) are highlighted on the electrical tomography profiles (Fig. 6).

The sedimentary fill of geoelectrical layer G1 was identified by Carrasco et al. (2015a), allowing the depositional system of G1 to be described as fluvial type. Proof of this is the contacts located in the seismic refraction profile (Fig. 8) that are associated with paleochannels.

Geoelectrical layer G2 is interpreted as genetically related to an alluvial fan supplied by marginal fluvioglacial flows from the Cuerpo de Hombre glacier. This delta fan is centred on the kame terrace where fluvioglacial flows originated (Fig. 5). Thus, there must have been a lacustrine paleoenvironment in the ND. This kind of environment progresses from the margin to the bottom of lake (in the ND located between ERT1 and ERT 2) as a Gilbert delta type, in which the sediments are packed like sigmoids identified as clinoforms in the ERT survey. As occurs in other similar contexts (Jalut et al., 2010; Turu et al., 2017), in the ND drainage was obstructed by the ice and/or the lateral moraine of the glacier. The low resistivity materials present in ERT 8 are therefore interpreted as fine-grained sediment at the bottom of this ice-dammed lake.

As also observed in other areas (Turu et al., 2017), the local base-level falls and the sedimentary facies change when the ice-damming comes to an end, producing diastems (unconformity surfaces, US). These erosive surfaces (ERT 8) mark the start of a new depositional sequence, initiating a Low System Tract (LST; Catuneanu, 2006). When the obstruction ceases, lacustrine sedimentation also stops, and an alluvial fan is initiated on the ND plain. The sigmoidal arrangement of clinoforms above the US in ERT 8 is an example of this sequence. These clinoforms are formed from a lateral accretion in the erosive entrenched channel, where migration of the sedimentary facies proceeds according to Walther's law (Vera, 1994).

The sedimentary evolution on this fluvial plain varies depending on changes in the local base level, which may be related to climatic factors (higher or lower moisture

contribution), glacial dynamics (retreat) or tectonics (greater subsidence or formation of erosive scarps).

In ND clinoforms display offlap evolution (ERT 8, Fig. 6.) This type of evolution is related to retrograde parasequences (Catuneanu, 2006). When maximum flooding is reached the finest grain-size sediments are deposited (Catuneanu, 2006), and promote low resistivities (Waxman and Smits, 1968) in ERT 8 (Fig. 6). This maximum flooding surface (msf) is known as a transgressive surface (TS, Catuneanu, 2006), and its identification is a key issue in sequence stratigraphy. Above this surface an aggradational sequence starts, present here on the left-hand side of unit G2 in ERT 8 (Fig. 6), and progressing to the end of unit G1 in ERT 8 (Fig. 6).

In the southernmost sector of the depression, a clear paraconformity is identified bringing resistive layers G1 and G2 into contact (ERT 1 and ERT 2). Here, layer G2 displays an onlap contact with layer G3 (ERT 1 and ERT 2). A possible explanation for this phenomenon is that tectonic subsidence facilitated the formation of this angular discontinuity between G2 and G3, and at the same time preserved the resistive layer G2 from erosion by G1. This interpretation is also supported by the fact that the sedimentary fill in ERT 2 would have been conditioned by greater subsidence on the western edge of the depression, forcing lateral accretion of the sigmoidal clinoforms in this direction. The lateral accretion and correlative vertical onlap surfaces, have no available space in ERT 8 and ERT 2, interpreted as a shallowing upward sequence. This sequence occurs at the start of the ERT 8 erosive surface (US, Fig. 6) which marks the end of the glacial obstruction in the ND. At that point alluvial fans progress over the ND plain (Fig. 5). A shallowing-upward sequence may indicate an accommodation lowering (Catuneanu, 2006), and thus a slight subsidence in the ND.

4.5. Navamuño basin geometry and tectonic controls

Taking into account the depth of the basement rock surface obtained in the VES, ERT sections and MRS, the Navamuño basin infill thickness was calculated and mapped (Fig. 9). These can be considered as minimum thickness values as the upper limit of the basement was not reached in some zones and so they were assigned the maximum penetration reached with the corresponding geophysical technique used. The calculated sediment volume for the basin is approx. $3.8 \cdot 10^6$ m^3, with a surface area 129,694 m^2.

The isopach map shows a depocentre over 60 m deep in the south and centre of the basin with a longitudinal NNE-SSW axis, parallel to the fractures defining the western edge of the basin. The maximum thickness variation gradients are the W and S borders, running NNE and ENE, respectively. These gradients, together with the morphostructural map (Fig. 4) suggest a clear structural control of ND basin at both edges by the NNE (PN Fault) and ENE (La Jara Fault) fracture families described in Section 2.0, above. To the N the infill thickness decreases more gradually, while the eastern boundary of the ND is more sharp (see onlap contacts in the right-hand side of ERT 1 and ERT 8, Fig. 6), limited by the lateral moraine.

Considering the morphology of the sedimentary infill provided by the ERT sections (Fig. 6, section 4.3), it was observed that unit G2 presents tilt in the centre of the depression (ERT 2), while G1 presents sedimentary accommodation towards the southern edge of the depression (ERT 7 and ERT 1). Geoelectrical layer G3 exhibits clearly defined limits (in ERT 7 and ERT 1) and is clearly confined by the rock substratum with structural limits in ERT 2 and ERT 8. All the above indicates a strong tectonic component which configures the limits of the depression and affects its sedimentary fill.

5. Discussion

The ND is one of the intermontain depressions forming the relief associated with the Hervás-Candelario corridor-type valleys, one of the main morphostructures of the W sector of the ICS. The evolution of these depressions is more complex than that of the great sedimentary transpressional basins (De Vicente et al., 2011) and is generally associated with NE-trending (NE-SW, NNE-SSW and N-S) strike-slip faults (Santanach et al., 1988, 2005; Carrasco and Pedraza, 1991; Santanach, 1994; Cabrera et al., 1996; Villamor et al., 1996; Alonso-Gavilán et al., 2004; Brum da Silveira, et al., 2009). Two examples of this morphotectonic configuration are the Valle del Jerte, 10 km to the east of the ND and linked to the AP fault (Carrasco and Pedraza 1991; Carrasco, 1997), and the series of depressions and platforms originating in the NE trend of the HC and Galisteo strike-slip faults and their associated faults (Moreno, 1991), including the PN fault which is mainly responsible for the ND morphostructure (Fig. 1).

Most of these ICS depressions occurring during the Paleogene /Lower Miocene, correlative with the early stages of tectonic reactivation of present relief. In general, are considered pull-apart type basins and in many cases aborted. Some of these were reactivated during the Plio-Pleistocene and Quaternary, hosting new deposits which present deformation structures catalogued as indicators of neotectonic activity (Brum da Silveira, 1990; Carrasco et al., 1991; Capote et al., 1996; Villamor et al., 1996, 2012; De Vicente, 2009; De Vicente et al., 2011).

Geophysical data obtained from the ND show a relatively deep depression, with sedimentary infill over 60 m thick. In the most surficial part of this fill (to depth 35 m) a coarsening-upward sedimentary sequence is found corresponding to geoelectrical layers G1 and G2, which from the available chronological data (Ruiz-Zapata et al., 2011; Carrasco et al., 2015a; Turu et al., 2018) corresponds to Upper Pleistocene and Holocene deposits. At depths of 35-45 m, the permeability and water content increase

considerably, but lower down both decrease rapidly to low permeability and low water content by depth 90 m.

From a genetic viewpoint, the deepest aquifer (below 45 m depth) should be associated with characteristic joints in rock with a weathering front above a depth of 60 m. The intermediate aquifer (at depths of 35-45 m) is the most productive and coincides with geoelectrical layer G3. This layer must be coarse grained to be so permeable and may correspond to arkosic deposits similar to described in depressions associated with the AP fault (Brum da Silveira, 1990; Capote et al., 1996; Villamor et al., 1996, 2012). In agreement with this data, the ND is similar to other small ICS depressions, which in genetic and evolutionary terms are associated with strike-slip faults and which, in some cases, have been interpreted as pull-apart type basins (Brum da Silveira, 1990; Carrasco and Pedraza, 1991; Capote et al., 1996; Villamor et al., 1996, 2012; De Vicente, 2009; De Vicente et al., 2011). The difference between the ND depression and these others is that the recent (Quaternary) sediments here are 30-35 m thick, compared with the 10-15 m obtained in other ICS intermontain depressions. Another distinctive characteristic of the ND, is that its evolution was linked to that of the Cuerpo de Hombre glacier during the Glacial Period in this area (Upper Pleistocene; ~MIS2), and the depression remained obstructed by moraines (and possibly by ice during the Maximum Ice Extent, MIE) during the stages of glaciatión.

In this context, both the subsidence dynamics and glacial-damming should be considered determining factors in the recent infill process of the ND. Although the data available from direct soundings is limited to the first 16 m of sediments (Carrasco et al., 2015a, Turu et al., 2018), the chrono-evolutionary data obtained from the study of the Cuerpo de Hombre paleoglacier (Carrasco et al., 2015b; Fig. 2) enable a chronological succession to be established for how this depression evolved throughout the Upper Pleistocene. The basin hydrologic regime was initially exorheic (drained by the Cuerpo de Hombre river) and was later obstructed by the glacier. The obstruction process started as ice-damming during the expansion stage of the glacier towards its MIE

(dated to 25.0 ± 1.3 ka; Carrasco et al., 2015b). Later, between 20.6 ± 2.5 ka and 17.8 ± 1.0 ka, the glacier built a wall-shaped lateral moraine (morainic Peripheral Deposits and Principal Moraine from Carrasco et al., 2015b; PD-M and PM, respectively, Figs. 2A, 2C) and blocked the eastern boundary of ND. This interpretation is based on an existing layer of alluvial fan deposits observed by Carrasco et al. (2015a) and Turu et al. (2018). The age obtained for the bottom of the peatland above the alluvial fan deposits is mid-Holocene (5160 ± 40 cal. yr BP, sample from 4.5 m depth, Ruiz-Zapata et al., 2011).

The path of the Cuerpo de Hombre glacier was carefully considered to explain the obstruction process. The current morphology of the Cuerpo de Hombre paleoglacier displays a confined valley between the two major lateral moraines (PM formations; Carrasco et al., 2015b). The right lateral moraine is attached to the bedrock slopes and displays a constant NW-SE direction throughout its upper and middle sector. The left lateral moraine also presents those same characteristics in its upper sector. However, its middle sector changes markedly. From the area where the moraine connects with the southern end of the ND, it is no longer confined in the bedrock relief, and runs in a NNW-SSE direction turning after to NNE-SSW parallel to PN fault (Figs. 2A, 4). These changes are maintained to the northern edge of the ND, giving rise to the wall-shaped lateral moraine relief which forms the boundary between the paleoglacier valley and the ND (Figs. 2A, 2C).

To explain the causes of this process, and most importantly, why the ice did not expand on to the ND plain during the advance stage towards its glacial maximum, three hypotheses can be established: (1) that the glacier in this zone was already in a reach with non-expansive stagnant flow; (2) that there was an ice flow process adapted to the morphological directives of a pre-glacial entrenched valley; and (3) that the ice flow was conditioned by the tectonic structure of the depression and its neotectonic evolution.

For the first hypothesis (1), from the data of this paleoglacier reconstruction during its Maximum Ice Extent (MIE) provided by Carrasco et al. (2015b) and revised and completed in this new research, the following can be established: (i) that the zone connecting the glacier and the ND plain starts at altitude 1600 m asl, at a distance of 1.7 km from the Equilibrium-Line Altitude (ELA, estimated at altitude 1966 m asl), and at 1.9 km from the glacier terminus which then was located at altitude 1260 m asl; and (ii) that the thickness of the glacial tongue ice in this reach was 50 m, much thicker than the ice in the stagnation zones close to glacier terminus or snout (with thickness 10-15 m). According to this data, the glacier tongue in this confluence zone was advancing in its middle-upper reach, and could have expanded on to the ND plain.

For the second hypothesis (2) and according to surface geomorphological data, there are no indicators of an existing pre-glacial entrenched valley which would have channelled the ice. The valley of the Cuerpo de Hombre paleoglacier and the ND are separated by the left lateral moraine of the PM formation, which originated a wall-shaped lateral moraine accumulating directly on both plains (Figs. 2A, 2C). In the reach where the paleoglacial valley and the ND appear connected, the plain of the ancient glacier bed (defined on the bedrock or with a thin layer of subglacial sediments of less than 2 m) and the ND plain are located at similar altitudes, presenting a gentle slope from the former to the latter (1585-1520 m asl and 1520-1480 m asl; maximum and minimum altitudes of the glacial valley bottom and the depression plain, respectively). A possible interpretation is therefore that in the pre-glacial stage both plains formed a single unit, later divided by the lateral moraine. Given the gradient between the two plains, in the glacier advance stages towards its maximum (MIE), previous to the development of the moraine (established from a first post-MIE retreat of the glacier, Carrasco et al., 2015b), the ice would have expanded towards the ND.

For the third hypothesis (3) and given that ND is associated with multiple faults, there is a solidly based argument for the existence of a tectonic structure in the relief (hypothesis 3) which conditioned the path of the glacial tongue.

Many studies have highlighted the impact of tectonic activity on the shape, location and path of glaciers, but also their capacity for adapting to tectonic structures (Clark, 1967, 1972; Clark et al., 2003; Gillespie and Clark, 2011; Glasser and Ghiglione 2009; Cotton et al., 2014; Bathrellos et al., 2017). In studies of ICS glacial morphology carried out to date (see here Pedraza and Carrasco, 2006), the general theory is that the glacial basins occupied structurally controlled pre-glacial river valleys, but indicators of the impact of tectonic structures or neotectonic activity on glacier dynamics have not been detected. By interpreting the data obtained from near surface geophysical research in ND, it can be deduced that the left lateral moraine of the Cuerpo de Hombre paleoglacier fossilized a small raised block which may initially have acted as the boundary between the glacier and the ND (Fig 8). In addition, and as previously described, in the sedimentary infill a series of structures is also detected which may be associated with neotectonic readjustment fault processes. According to these data, the evolutive sequence of ND, and the effect of these processes on the path of the Cuerpo de Hombre glacier, can be established as detailed below.

The depression obstruction process may have already been initiated by the glacier tongue during its expansion phase towards the maximum extent (MIE) and was later consolidated by the moraines. In this context, still supposing that the sedimentation rate in the obstructed cuvette was very low or nil during the glacial phase and the majority of the sediments detected by geophysics were all pre-glacier, the 16 m of sediments of post-glacier fill detected with direct test bores (Carrasco et al., 2015a; Turu et al., 2018) imply the elevation of the depression plain which: (1) must have fossilized almost completely the formation of dispersed erratic boulders (PD-B; Carrasco et al., 2015b, Fig. 2C); and (2) reveals that the base of the depression at the onset of the glacial stage was some 15-30 m (extreme north and south, respectively) lower than the floor of the glacial valley. Therefore, there was evidently a sufficient longitudinal gradient of the terrain for the glacier to maintain its trajectory according to the line of minimum slope. However, and as has been shown, after a slight advance

towards the depression, the glacier made an abrupt turn and came to a standstill at its margin.

According to these data, it can be established that: (1) at that point the configuration of the relief on the bottom of the depression must have been very different and acted as a threshold controlling the direction of the ice flow; and (2) given that the present base of the depression is at lower elevations than the floor of the glacial valley and hosts the sediments corresponding to the obstruction process, the only possible explanation for this process is the sinking of the depression during these infill phases.

In relation to this sinking of the sedimentary depression, the suggestions are that it was caused by gravitational movements (rotation platform) or by differential movements between blocks limited by faults (tectonic readjustments). Both the data provided by geophysics and the regional context data are sufficient arguments to consider that the most probable process was the latter. The onlap contact shown in geoelectrical layer G2 in ERT 1, and geoelectrical layer G1 in ERT 7, are indicators of syntectonic sedimentation in ND (Fig. 6). The same occurs with geoelectrical layer G3 (ERT 1, ERT 3 and ERT 7) which is limited by high dip faults in ERT 2 and ERT 8 (Fig. 6). This rock threshold where the lateral moraine of the Cuerpo de Hombre paleoglacier is found, corresponds to a raised block, and would have acted as a limit to the path of the ice.

On the other hand, although the ICS and the centre of the Iberian Peninsula are classified as zones of very low to moderate seismicity, (IGN, 2016), from analysing the current river network of the ICS and other related areas in the central Iberian Meseta, multiple indicators emerge of structural control, and of recent and current impact of neotectonics with paleoseismic structures originating throughout the Pleistocene (Pedraza, 1976; Carrasco et al., 1991; Silva et al., 1988; Pol et al., 1989; De Vicente et al., 2007, 2011; Garzón et al., 2014). In this context, the proposed model for the route followed by the paleoglacier can be considered coherent.

6. Conclusions

The ND is a ~30 ha pseudo-endorheic flat basin over granitic bedrock with water ponding associated with the PN fault, a NNE-SSW trending Variscan strike-slip fault correlated with the series of strike-slip faults described along the ICS. In the geomorphological and geophysical studies carried out in this research, a sedimentary infill over 60 m thick has been proven. This agrees with that established in recent previous investigations and allows us to catalog the ND as the largest and deepest sedimentary basin of the ICS associated with glacial processes (glacier obstruction or overdeepening).

Geophysical surveys have been critical in identifying the infill depth in the depression and the geometrical relationships existing in the rock substrata. This information, together with that provided by the surficial geology and geomorphology, supports the hypothesis that: (1) ND can be correlated with the small sedimentary basins located along the Variscan strike-faults described in the Iberian Massif and classified as an intermontain tectonic basin with primary origin due to a transtensional process in the PN strike-slip fault during the stages of reactivation of the ICS (Oligocene-lower Miocene); (2) part of the sedimentary infill is related to the contribution made at the time by the Cuerpo de Hombre glacier meltwater through a system of marginal flows; and (3) both in the path of the glacier and in the sedimentary infill of the ND correlative to the glacial and postglacial stages, we have detected indicators of neotectonic activity.

The Cuerpo de Hombre paleoglacier had a marked influence on sedimentary evolution in the ND, as it was responsible for the shift from an exorheic hydrologic regime to a semi-endorheic regime with ponding. From the available data, this process took place during the maximum glacial advance stage (approx. 25.0 ± 1.3 ka BP) and continued at least until silting-up occurred during the Holocene. Neotectonic

readjustment has continued from the last glacial cycle to the present day. However, the post-glacial sedimentary infill in the depression presents a shallowing-upward sequence, which is considered an indicator of decreasing subsidence.

Acknowledgements

This work was supported by the Spanish Ministry of Economy and Competitiveness (Projects CGL2013-44076-P and CGL2016-78380-P). The authors also wish to acknowledge the help and assistance of the Regional Environment Department (JCyL) and the Local Authority in the village of Candelario. We also thank to the Editor and the reviewers, for their helpful comments and constructive suggestions that greatly improved this manuscript.

References

Abel-Schaad, D., Pulido, F., López-Sáez, J.A., Alba Sánchez, F., Nieto Lugilde, D., Franco Múgica, F., Pérez-Díaz, S., Ruiz Zapata, M.B., Gil García, M.J., Dorado Valiño, M., 2014. Persistence of tree relicts in the Spanish Central System through the Holocene. Lazaroa 35, 107-131.

Alonso-Gavilán, G., Armenteros, I., Carballeira, J., Corrochano, A., Huerta, P., Rodríguez, J. M., 2004. Cuencas cenozoicas del Macizo Ibérico. In Vera, J.A. (Ed.), Geología de España. SGE-IGME. Madrid, Spain, pp. 581-584.

Anon, 1977. The description of rock masses for engineering purposes: Report by the Geological Society Engineering Group Working Party. Q. J. Eng. Geol. Hydrogeol. 10, 355-388.

Barker, R., 1992. A simple algorithm for electrical imaging of the subsurface. First Break 10, 53 – 62.

Bathrellos, G., Skilodimou, H., Maroukian, H., 2017. The significance of tectonism in the glaciations of Greece. Geological Society, London, Special Publications 433, 237-250.

Behroozmand, A.A., Keating, K., Auken, E., 2015. A Review of the Principles and Applications of the NMR Technique for Near-Surface Characterization. Surv. Geophys. 36, 27-85.

Bellido-Mulas, F. (Ed.), 2006. Mapa Geológico de Cabezuela del Valle, 1:50 000. Map 576. Instituto Geológico y Minero de España. Madrid, Spain. http://www.igme.es

Ber, A., 2009. Vertical stress of the pleistocene continental glaciers and its hypothetical evidence in present relief of Northern Europe. Polish Geol. Inst. Spec. Pap. 25, 7–12.

Bhattacharya, P.K., Patra, H.P. (Eds.), 1968. Direct current geoelectric sounding, principles and interpretation. Elsevier, Amsterdam, Netherlands.

Bobachev, A.A, Shevnin, V.A., Modin, I.N., 2003. IPI2WIN version 3.0.1e. http://geophys.geol.msu.ru/ipi2win.htm.

Bordonau, J., 1992. Els Complexos glàcio-lacustres relacionats amb el darrer cicle glacial als Pirineus. Ph.D. Thesis, Barcelona Univ., Spain.

Brum da Silveira, A., 1990. Neotectónica e Sismotectónica da Região Vidigueira–Moura. Ph.D. Thesis, Univ. Lisboa, Portugal.

Brum da Silveira, A., Cabral, J., Perea, H., Ribeiro, A., 2009. Evidence for coupled reverse and normal active faulting in W Iberia. The Vidigueira-Moura and Alqueva faults (SE Portugal). Tectonophysics 474, 184–199.

Cabral, J., 1995. Neotectónica em Portugal Continental. Memórias do Instituto Geológico e Mineiro 31, Lisboa, Portugal.

Cabral, J., 2012. Neotectonics of mainland Portugal: state of the art and future perspectives. J. Iber. Geol. 38, 71–84.

Cabrera, L., Ferrús, B., Sáez, A., Santanach P., Bacelar J., 1996. Onshore Cenozoic strike-slip basins in NW Spain. In: Friend, P. F., Dabrio, C.J. (Eds), Tertiary Basins of Spain. Cambridge Univ. Press, New York, USA, pp. 247-254.

Capote, R., Villamor, P., Tsige, M., 1996. La tectónica alpina de la Falla de Alentejo-Plasencia (Macizo Hespérico). Geogaceta 20, 921–924.

Carrasco, R.M., 1997. Estudio Geomorfológico del Valle del Jerte (Sistema Central Español): secuencia de procesos y dinámica morfogenética actual. Ph.D. Thesis, Complutense Univ. Madrid, Spain.

Carrasco, R.M., Pedraza, J., 1991. Historia morfodinámica de la Falla de Plasencia en el Valle del Jerte. In: Actas de Gredos, V Jornadas de Verano de La Sierra de Gredos, Boletín Universitario 11, UNED, Ávila, Spain, pp. 17–30.

Carrasco, R.M., Pedraza, J., Rubio, J.C., 1991. Actividad neotectónica cuaternaria en el Valle del Jerte. Cuaternario y Geomorfología 5, 15–25.

Carrasco, R.M., Pedraza, J., Domínguez-Villar, D., Willembring, J., Razola, L., Edwards, L., Wang, Y., Fairchild, I.J., Baker, A., Ruiz-Zapata, M.B., Centeno, J., 2009. Chronology and causes of the Last Glacial Maximum in Spanish Central System: the project methodology. 7th International Conference on Geomorphology (ANZIAG). Conference Abstracts, Melbourne, Australia.

Carrasco, R.M., Pedraza, J., Domínguez-Villar, D., Villa, J., Willenbring, J.K., 2013. The plateau glacier in the Sierra de Béjar (Iberian Central System) during its maximum extent. Reconstruction and chronology. Geomorphology 196, 83–93.

Carrasco, R.M., Sánchez, J., Muñoz-Martín, A., Pedraza, J., Olaiz, A.J., Ruiz-Zapata, B., Abel-Schaad, D., Merlo, O., Domínguez-Villar, D., 2015a. Caracterización de la geometría de la depresión de Navamuño (Sistema Central Español) aplicando técnicas geofísicas. Geogaceta 57, 39–42.

Carrasco, R.M., Pedraza, J., Domínguez-Villar, D., Willenbring, J.K., Villa, J., 2015b. Sequence and chronology of the Cuerpo de Hombre paleoglacier (Iberian Central System) during the last glacial cycle. Quat. Sci. Rev. 129, 163–177.

Catuneanu, O., 2006. Principles of Sequence Stratigraphy. Elsevier Science, Amsterdam, Netherlands.

Centeno, J.D., Brell, J.M., 1987. Características de las alteraciones de las Sierras de Guadarrama y Malagon (Sistema Central Español). Cuaderno Lab. Xeolóxico de Laxe 12, 79-87.

Clark, M.M., 1967. Pleistocene glaciation of the drainage of the West Walker River, Sierra Nevada, California. Ph.D. Dissertation, Stanford, Stanford University, USA.

Clark, M.M., 1972. Range-front faulting: cause of anomalous relationships among moraines of the eastern slope of the Sierra Nevada, California. Geol. Soc. Am. Abstr. Programs 4, 137.

Clark, D., Gillespie, A.R., Clark, M.M., Burke, R.M., 2003. Mountain glaciations of the Sierra Nevada. In: Easterbrook, D.J. (Ed.), Quaternary Geology of the United States. International Quaternary Association: INQUA 2003. Field Guide Volume. XVI INQUA Congress. Desert Research Institute, Reno, USA, pp. 287–312.

Cotton, M.M., Bruhn, R.L., Sauber, J., Burgess, E., Forster, R.R., 2014. Ice surface morphology and flow on Malaspina Glacier, Alaska: Implications for regional tectonics in the Saint Elias orogen. Tectonics 33, 558–595.

Dearman, W.R., 1978. Weathering classification in the characterization of rock: a revision. Bull. Int. Assoc. Eng. Geol. 18, 123–128.

De Brujne, C.H., Andriessen, P.A.M., 2002. Far field effects of Alpine plate tectonism in the Iberian microplate recorded by faultrelated denudation in the Spanish central system. Tectonophysics 349,161-184.

Descloitres, M., Ruiz, L., Sekhar, M., Legchenko, A., Braun, J.J., Mohan Kumar, M.S., Subramanian, S., 2008. Characterization of seasonal local recharge using electrical resistivity tomography and magnetic resonance sounding. Hydrol. Process. 22, 384–394.

De Vicente, G., 2009. Partición de la deformación cenozoica intraplaca en el Sistema Central. Geogaceta 46, 23-26.

De Vicente, G., Vegas, R., 2009. Large-scale distributed deformation controlled topography along the western Africa–Eurasia limit: tectonic constraints. Tectonophysics 474, 124-143.

De Vicente, G., Vegas, R., Muñoz Martín, A., Silva, P.G., Andriessen, P., Cloetingh, S., González Casado, J.M., Van Wees, J.D., Álvarez, J., Carbó, A., Olaiz, A., 2007. Cenozoic thick-skinned deformation and topography evolution of the Spanish Central System. Glob. Planet. Change 58, 335–381.

De Vicente, G., Cloetingh, S., Van Wees, J.D., Cunha, P.P., 2011. Tectonic classification of Cenozoic Iberian foreland basins. Tectonophysics 502, 38–61.

Foroutan, M., Vilanova, S., Heleno, S., Pinto, L., Far, A.S., Falcao-Flor, A., Canora, C., Pina, P., Vieira, G., Fonseca, J., 2016. New evidence for large earthquakes in mainland Portugal: paleoseismology of the Lower Tagus Valley fault. 35th General Assembly of the European Seismological Commission. ESC2016-489-1.

Franco-Múgica, F., 1995. Estudio palinológico de turberas holocenas en el Sistema Central: reconstrucción paisajística y acción antrópica. Ph.D. Thesis, Univ. Autónoma. Madrid, Spain.

Garate, J., Martin-Davila, J., Khazaradze, G., Echeverria, A., Asensio, E., Gil, A.J., de Lacy, M.C., Armenteros, J.A., Ruiz, A.M., Gallastegui, J., Alvarez-Lobato, F., Ayala, C., Rodríguez-Caderot, G., Galindo-Zaldívar, J., Rimi, A., Harnafi, M., 2015. Topo-Iberia project: CGPS crustal velocity field in the Iberian Peninsula and Morocco. GPS Solutions, 19, 287-295.

Garzón, G., Garrote, J., Tejero, R., 2014. La integración de la red fluvial del margen norte del río Tajo. El papel de las depresiones cenozoicas. In: Schnabel, S., Gómez-Gutiérrez, A. (Eds.), Avances de la Geomorfología en España 2012-2014. Universidad de Extremadura, SEG, Cáceres, Spain, pp. 393-396.

Génova, M., Gómez-Manzaneque, F., Martínez-García, F., Postigo-Mijarra, J.M., 2016. Early Holocene vegetation in the Ayllón Massif (Central System Range, Spain) based on macroremains. A paleoecological approach. Palaeogeogr. Palaeoclimatol. Palaeoecol. 441, 811–822.

Gillespie, A.R., Clark, D.H., 2011. Glaciations of the Sierra Nevada, California, USA. In: Ehlers, J., Gibbard, P.L., Hugges, P.D. (Eds.), Quaternary Glaciations – Extent and Chronology. Elsevier, Amsterdam, Netherlands, pp. 447-462.

Glasser, N.F., Ghiglione, M.C., 2009. Structural, tectonic and glaciological controls on the evolution of fjord landscapes. Geomorphology 105, 291–302.

Grunewald, E., Knight, R., 2011. The effect of pore size and magnetic susceptibility on the surface NMR relaxation parameter T_2*. Near Surface Geophysics 9, 169-178.

Hausmann, J., Steinel, H., Kreck, M., Werban, U., Vienken, T., Dietrich, P., 2013. Two-dimensional geomorphological characterization of a filled abandoned meander using geophysical methods and soil sampling. Geomorphology 201, 335–343.

Herrero-Simón, R., 2003. Anasim code V.6.0; Internal software from the Nuclear and Physics Engineering Department of the Universitat Politècnica de Catalunya (UPC), Terrassa, Spain.

Herrero-Simón, R., 2007. Simusism code V.2.0; Internal software from the Nuclear and Physics Engineering Department of the Universitat Politècnica de Catalunya (UPC), Terrassa, Spain.

Hertrich, M., 2008. Imaging of groundwater with nuclear magnetic resonance. Prog. Nucl. Magn. Reson. Spectrosc. 53, 227–248.

IGN, 2016. Mapas de sismicidad y peligrosidad. Instituto Geográfico Nacional, Spain. http://www.ign.es

Jalut, G., Turu, V., Dedoubat, J.J., Otto, T., Ezquerra, J., Fontugne, M., Belet, J.M., Bonnet, L., de Celis, A.G., Redondo-Vega, J.M., Vidal-Romaní, J.R., Santos, L., 2010. Palaeoenvironmental studies in NW Iberia (Cantabrian range): Vegetation

history and synthetic approach of the last deglaciation phases in the western Mediterranean. Palaeogeogr. Palaeoclimatol. Palaeoecol. 297, 330–350.

Lange, G., Yaramanci, U., Meyer, R., 2007. Surface Nuclear Magnetic Resonance. In: Knödel, K., Lange, G., Voigt, HJ. (Eds.), Environmental Geology. Springer Berlin Heidelberg, Germany, pp. 403–430.

Legchenko, A.V., Shushakov, O.A., 1998. Inversion of surface NMR data. Geophysics, 63 (1), 75-84.

Loke, M.H., Barker, R.D., 1996. Rapid least-squares inversion of apparent resistivity pseudosections by a quasi-Newton method. Geophys. Prospect. 44, 131-152.

Loke, M.H., Wilkinson, P.B, Chambers, J.E., 2010. Parallel computation of optimized arrays for 2-D electrical imaging surveys. Geophys. J. Int. 183, 1302-1315.

López-Sáez, J.A., Abel-Schaad, D., Pérez-Díaz, S., Blanco-González, A., Alba-Sánchez, F., Dorado, M., Ruiz-Zapata, B., Gil-García, M.J., Gómez-González, C., Franco-Múgica, F., 2014. Vegetation history, climate and human impact in the Spanish Central System over the last 9000 years. Quat. Int. 353, 98–122.

López-Sáez, J.A., Abel-Schaad, D., Robles-López, S., Pérez-Díaz, S., Alba-Sánchez, F., Nieto-Lugilde, D., 2016. Landscape dynamics and human impact on high-mountain woodlands in the western Spanish Central System during the last three millennia. JASREP 9, 203–218.

Maillet, R., 1947. The fundamental equations of electrical prospecting. Geophysics 12, 529-556.

Mejías, M., Plata, J., 2007. General concepts in Hydrogeology and Geophysics related to MRS. Bol. Geol. y Min. 118, 423–440.

Mendes-Victor, L., Oliveira, C.S., Azevedo, J., Ribeiro, A. (Eds.), 2009. The 1755 Lisbon Earthquake: Revisited. Springer, Netherlands.

Molina-Ballesteros, E., García-González, M.T., Espejo, R., 1991. Study of Paleoweathering on the Spanish Hercynian basement Montes de Toledo (Central Spain). Catena 18, 345-354.

Molina-Ballesteros, E., García-Talegón, J., Vicente-Hernández, M. A., 1994. Las paleoalteraciones sobre el zócalo hercínico ibérico. Aproximación a una interpretación regional a partir de perfiles españoles. Cuaderno Lab. Xeolóxico de Laxe 19, 261-271.

Molina-Ballesteros, E., García-Talegón, J., Vicente-Hernández, M.A., 1997. Palaeoweathering profiles developed on the Iberian Hercynian Basement and their relationship to the oldest Tertiary surface in central and western Spain. Geol. Soc. London, Spec. Publ. 120, 175–185.

Moreno, F., 1991. Superficies de erosión y tectónica neógena en el extremo occidental del Sistema Central español. Geogaceta 9, 47-50.

Muñoz Martín, A., De Vicente, G., Olaiz, A., Antón, L., Vegas, R., Granja, J.L., 2012. Mapa de esfuerzos activos en línea de la Península Ibérica a partir de Mecanismos Focales calculados desde el Tensor de Momento Sísmico. Geotemas 13, 1-4.

Olaiz, A.J., Muñoz-Martín, A., De Vicente, G. Vegas, R., Cloeting, S., 2009. Oblique strain partitioning and transpression on an inverted rift: The Castilian Branch of the Iberian Chain. Tectonophysics 470, 224-242.

Olvmo, M., Johansson, M., 2002. The significance of rock structure, lithology and pre-glacial deep weathering for the shape of intermediate-scale glacial erosional landforms. Earth Surf. Process. Landforms 27, 251–268.

Palmer, D., 1980. The generalized reciprocal method of seismic refraction interpretation. Society of Exploration Geophysicists, Tulsa, USA.

Pedraza, J., 1976. Algunos procesos morfogenéticos recientes en el valle del río Alberche (Sistema Central Español). La depresión de Aldea del Fresno-Almorox. Bol. Geol. y Min. 87, 1–12.

Pedraza, J., 1994. Sistema Central. In: Gutiérrez Elorza, M. (Ed.), Geomorfología de España. Rueda, Spain, pp. 63–100.

Pedraza, J., 2012. Late Pleistocene glacial evolutionary stages in the Spanish Central System. Quat. Int. 279–280, 371–372.

Pedraza, J., Carrasco, R. M., 2006, El glaciarismo pleistoceno del Sistema Central. AEPECT, 13 (3), 278-288.

Pedraza, J., Carrasco, R.M., Domínguez-Villar, D., Villa, J., 2013. Late Pleistocene glacial evolutionary stages in the Gredos Mountains (Iberian Central System). Quat. Int. 302, 88–100.

Pèlachs, A., Julià, R., Pérez-Obiol, R., Burjachs, F., Expósito, I., Yll, R., Vizcaino, A., Turu, V., Soriano, J.M., 2011. Dades paleoambientals del complex glaciolacustre de l'estany de Burg durant el Tardiglacial (Vall Farrera, Pallars Sobirà). In: Turu, V. and Constante, A. (Eds.), Simposio de Glaciarismo: El Cuaternario en España y áreas afines, Avances en 2011. Fundació Marcel Chevalier- AEQUA. Andorra la Vella, pp. 40–50.

Pellicer, X.M., Zarroca, M., Gibson, P., 2012. Time-lapse resistivity analysis of Quaternary sediments in the Midlands of Ireland. J. Appl. Geophys. 82, 46–58.

Plata, J.L., Rubio, F.M., 2008. The use of MRS in the determination of hydraulic transmissivity: The case of alluvial aquifers. J. Appl. Geophys. 66, 128–139.

Pol, C., Sánchez del Corral, A., Carballeira, J., 1989. Neotectónica en la cuenca del alto Tormes (Sistema Central, Ávila): Influencia en la morfología fluvial. Geogaceta 6, 90–94.

Prasicek, G., Larsen, I.J., Montgomery, D.R., 2015. Tectonic control on the persistence of glacially sculpted topography. Nat. Commun. 6, 8028.

Reynolds, J.M., 2011. An Introduction to Applied and Environmental Geophysics. Wiley-Blackwell, Chichester, UK.

Rodríguez Fernández, L.R.; Oliveira, J.T. (Ed.), 2015. Mapa Geológico de la Península Ibércia, Baleares y Canarias a escala 1:1.000.000. Instituto Geológico y Minero de España. Madrid, Spain. http://www.igme.es

Rubiales, J.M., García-Amorena, I., Génova, M., Gómez Manzaneque, F., Morla, C., 2007. The Holocene history of highland pine forests in a submediterranean mountain: the case of Gredos mountain range (Iberian Central range, Spain). Quat. Sci. Rev. 26, 1759–1770.

Rubio, J.C., 1990. Geomorfología y Cuaternario de las sierras de la Nava y Béjar (Sistema Central Español). PhD Thesis, Complutense Univ., Madrid, Spain.

Ruiz-Zapata, M.B., Carrasco, R.M., Gil-García, M.J., Pedraza, J., Razola, L., Domínguez- Villar, D., Gallardo, J.L., 2011. Dinámica de la vegetación durante el Holoceno en la Sierra de Gredos (Sistema Central Español). Bol. R. Soc. Esp. Hist. Nat. 105, 109-123.

Salazar-Rincón, A., Mata-Campo, P., Rico-Herrero, M.T., Valero-Garcés, B.L., Oliva-Urcia, B., Ibarra, P., Rubio, F.M., 2013. El paleolago de La Larri (Valle de Pineta, Pirineos): Significado en el contexto del último máximo glaciar en el Pirineo. Cuadernos de Investigación Geográfica 39, 97-116.

Santanach, P., 1994. Las cuencas terciarias gallegas en la terminación occidental de los relieves pirenaicos. Cuad. Lab. Xeol. Laxe 19, 57-71.

Santanach, P., Baltuille, J.M., Cabrera, L., Monge, C., Sáez, A., Vidal-Romaní, J.R. 1988. Cuencas terciarias gallegas relacionadas con corredores de falla direccionales. II Congreso Geológico de España, IGME, Granada, Spain, pp. 123-133.

Santanach, P, Ferrús, B., Cabrera, L., Sáez, A., 2005. Origin of a restraining bend in an evolving strike-slip system: The Cenozoic As Pontes basin (NW Spain). Geol. Acta 3, 225–239.

Sanz-Donaire, J.J., 1979. El Corredor de Béjar. Instituto de Geografía aplicada. CSIC, Madrid, Spain.

Schrott, L., Hördt, A., Dikau, R. (Eds.), 2003. Geophysical applications in geomorphology. Zeitschr. f. Geomorphologie Supplementbände, 132, 190S.

Sheehan J.R., Doll W.E., Mandell W.A., 2005. An evaluation of methods and available software for seismic refraction tomography analysis. J. Environ. Eng. Geophysics. 10, 21–34.

Sheriff, E.R., Geldart, L.P., 1991. Exploración sismológica. Volumen II. Procedimientos e interpretación de datos. Limusa, México.

Shushakov, O.A., Legchenko, A.V., 1994. Groundwater proton magnetic resonance in the horizontally stratified media of different electrical conductivity. Geol. Geophys. 35, 130-136 (in Russian).

Silva, P., Goy, J.L., Zazo, C., 1988. Evolución Geomorfológica de la confluencia de los ríos Jarama y Tajuña durante el cuaternario (Cuenca de Madrid, España). Cuaternario y Geomorfología 2, 125–133.

Turu, V., 1999. Aplicación de diferentes técnicas geofísicas y geomecánicas para el diseño de una prospección hidrogeológica de la cubeta de Andorra, (Pirineo Oriental): implicaciones paleohidrogeológicas en el contexto glacial andorrano. In: Actualidad de las técnicas geofísicas aplicadas en hidrogeologia. ITGE-IGME, Madrid, Spain, pp. 203-210.

Turu, V., 2012. Surface NMR survey on Hansbreen Glacier, Hornsund, SW Spitsbergen. Landform Analysis 21, 57-74.

Turu, V., Boulton G. S., Ros X., Peña-Monne J. L., Marti-Bono C., Bordonau J., Serrano-Cañadas E., Sancho-Marcén, C., Constante-Orrios A., Pous J., Gonzalez-Trueba J. J., Palomar J., Herrero-Simón, R., García-Ruiz, J. M., 2007. Structure des grands bassins glaciaires dans le nord de la Péninsule Ibérique: comparaison entre les vallées d'Andorre (Pyrénées Orientales), du Gállego (Pyrénées Centrales) et du Trueba (Chaîne Cantabrique). Quaternaire 18, 309–325.

Turu, V., Ventura, J., Ros, X., Pélachs, A., Vizcaino, A., Soriano, J.M., 2011. Geomorfologia glacial del tram final de la Noguera Pallaresa i riu Flamicell (Els Pallars). In: In: Turu, V., Constante-Orrios, A. (Eds.), Simposio de glaciarismo:

El Cuaternario en España y áreas afines, avances en 2011. Fundació Marcel Chevalier-AEQUA, Andorra la Vella, pp. 37-43.

Turu, V., Calvet, M., Bordonau, J., Gunnell, Y., Delmas, M., Vilaplana, J.M., Jalut, G., 2017. Did Pyrenean glaciers dance to the beat of global climatic events? Evidence from the Würmian sequence stratigraphy of an ice-dammed palaeolake depocentre in Andorra. Geol. Soc. London, Spec. Publ. 433, 111-136.

Turu, V., Carrasco, R.M., Pedraza, J., Ros, X., Ruiz-Zapata, B., Soriano-López, J.M., Mur-Cacuho, E., Pélachs-Mañosa, A., Muñoz-Martín, A., Sánchez, J., Echeverria-Moreno, A., 2018. Late glacial and post-glacial deposits of the Navamuño peatbog (Iberian Central System): Chronology and paleoenvironmental implications. Quat. Int. 470, 82-95.

Udías, A., López Arroyo, A., 2009. The Lisbon Earthquake of 1755 in Spanish Contemporary Authors. In Mendes-Victor, L., Oliveira, C.S., Azevedo, J., Ribeiro, A. (Eds.), The 1755 Lisbon Earthquake: Revisited. Springer, Dordrecht, Netherlands, pp. 7-24.

Vail, P.R., Colin, J.P., du Chene, R.J., Kuchly, J., Mediavilla, F., Trifilieff, V., 1987. La stratigraphie sequentielle et son application aux correlations chronostratigraphiques dans le Jurasique du basin de Paris. B. Soc. Geol. Fr. 8, 1301-1321.

Vázquez, J.T., Vegas, R., Barranco, L.M., 1987. Rasgos morfológicos de la depresión del Burguillo (Sistema Central Español) y su relación con deformaciones recientes. Cuaternario y Geomorfología 1, 295–308.

Vera, J.A., 1994. Estratigrafía, Principios y Métodos. Ed. Rueda, Madrid, Spain.

Vilaplana, J.M., Casas, A., 1983. Las cubetas de sobreexcavación glacial de Bono y Barruera (Alta Ribagorça, Pirineo Central). Cuad. Lab. Xeol. de Laxe 6, 283-309.

Villamor, P., Capote, R., Tsige, M., 1996. Actividad neotectónica de la Falla de Alentejo-Plasencia en Extremadura (Macio Hespérico). Geogaceta 20, 925–928.

Villamor, P., Capote, R., Stirling, M.W., Tsige, M., Berryman, K.R., Martínez-Díaz, J.J., Martín-González, F., 2012. Contribution of active faults in the intraplate area of Iberia to seismic hazard: The Alentejo-Plasencia Fault. J. Iber. Geol. 38, 85–111.

Villaseca, C., 2003. Sobre el origen del batolito granítico del Sistema Central Español. Bol. R. Soc. Esp. Hist. Nat. 98, 23-39.

Villaseca, C., Barbero, l., Herreros, V., 1999. A re-examination of the typology of peraluminous granite-types in intracontinental orogenic belts. Trans. R. Soc. Edinb. Earth Sci. 89, 113-119.

Vouillamoz, J.M., Baltassat, J.M., Girard, J.F., Plata, J., Legchenko, A., 2007. Hydrogeological experience in the use of MRS. Bol. Geol. y Min. 118, 531–550.

Walsh, D. O., 2008. Multi-channel surface NMR instrumentation and software for 1D/2D groundwater investigations. J. Appl. Geophys. 66, 140-150.

Watanabe, T., Matsuoka, T., Ashida, Y., 1999. Seismic traveltime tomography using Fresnel volume approach. SEG Technical Program Expanded Abstracts 1999, 1402-1405.

Waxman, M.H., Smits, L.J.M., 1968. Electrical conductivities in oil-bearing shaly sands. SPE Journal 8, 107–122.

Weichmann, P.B., Lavely, E.M., Ritzwoller, M.H., 2000. Theory of surface nuclear magnetic resonance with application to geophysical imaging problems. Phys. Rev. E. 62, 1290–1312.

Yamakawa, Y., Kosugi, K., Masaoka, N., Sumida, J., Tani, M., Mizuyama, T., 2012. Combined geophysical methods for detecting soil thickness distribution on a weathered granitic hillslope. Geomorphology 145-146, 56–69.

Yanites, B.J., Ehlers, T.A., 2012. Global climate and tectonic controls on the denudation of glaciated mountains. Earth Planet. Sci. Lett. 325-326, 63–75.

Yaramanci, U., 2000. Surface Nuclear Magnetic Resonance (SNMR) - A new method for exploration of ground water and aquifer properties. Ann. Di Geofis. 43, 1159-1175.

Zohdy, A.A.R., 1989. A new method for automatic interpretation of Schlumberger and Wenner sounding curves. Geophysics 54, 244–253.

Figure captions

Fig. 1. Geological location of the study area. Geological diagram based on the *Mapa geológico de la Península Ibérica, Baleares y Canarias.* Scale 1: 1.000.000 (Rodríguez Fernández and Oliveira, 2015).

Fig. 2. A) Stages of retreat in Cuerpo de Hombre paleo-glacier and chronologies ka BP (based on Carrasco et al., 2015b). 3D image of the Navamuño Depression and Cuerpo de Hombre paleoglacier using ArcScene 10.4 and PNOA-2014 orthophoto (http://www.ign.es). B) General view of the Navamuño Depression photographed from its SW boundary facing NE. C) Panoramic view of the Cuerpo de Hombre valley and Navamuño depression. Green arrow indicate glacier path. Letters indicate the morphostratigraphic formations (Carrasco et al., 2015b): PD peripheral deposits (B-boulders and M-moraine); PM principal moraine; ID internal deposits (M1 to M4, recessional moraines).

Fig. 3. A) Location of field work carried out in the Navamuño Depression (image: DTM5 m, http://www.ign.es). B) Seismic array deployed in the depression distal zone. C) MRS1 data collection in the centre of the peat bog. D) Profile ERT9 transversal to the depression and drawn perpendicular to the Cuerpo de Hombre paleoglacier lateral moraine.

Fig. 4. Fracture network associated with Navamuño tectonic depression.

Fig. 5. Electrical resistivity curves from Vertical Electrical Sounding data. Main resistivity layers (G1 to G3). Layer G1 corresponds to the shallower geoelectrical layer. Resistivity from layer G2 is quite variable in resistivity and is interpreted as corresponding to alluvial fan and floodplain deposits. Layer G3 corresponds to older

sedimentary deposits present in deeper positions in the Navamuño depression, but the G3 geoelectrical layer is also perched beneath the kame deposits. Resistivity anomalies, as in VES 8 and VES 7, occur when electrodes sharply cross basement and sedimentary deposits. If this is not the case and a transition exists between granite and the sedimentary infill, then it is difficult to identify the depth of the basement (VES 4 and VES 6).

Fig. 6. ERT tomography and geological interpretation including VES and MRS positions.

Fig. 7. Magnetic Resonance Sounding data and inversion results. Solid line-squares: groundwater signal. Circles: electromagnetic noise.

Fig. 8. Interpretation of the seismic profile using P-wave velocity and thickness of deducted seismic units. Seismic velocity is inversely related to the slope of the linear regression. Anomalies in PS1 and PS3 time-distance graphics are related with vertical jumps (erosive surfaces or sharp facies changes). All numbers that overlap geological materials are seismic velocities (in meters per second). NRZ = Non-Refraction Zone from an over-pressurized aquifer. Refractions coming from a denser terrain on PS1 (D) are interpreted as being related to the bedrock basement. On the opposite side of the profile (PS4), bedrock basement is located below the moraine at shallow depth.

Fig. 9. Isopach map of the Navamuño Basin infill obtained from interpolating the thicknesses calculated in the geophysical data. In the zones where the upper limit of the granitic basement was not reached, a minimum thickness has been assigned, equal to the penetration reached with each technique. The infill isopachs are superimposed on the LiDAR topography produced by the IGN. The interpolation has been carried out using kriging at grid resolution of 5 m with a linear variogram, based

on all the data. The grid was then blanked outside the zone with zero thickness. To improve the isopach map, we have used the cartographic boundary of the basin infill, adding these data with zero thickness to the thickness values calculated using geophysical methods.

Table 1. Topographic parameters of the central point of the Magnetic Resonance Sounding (MRS) profiles.

	MRS 1	MRS 2
Latitude (DD)	40.321147	40.321109
Longitude (DD)	-5.778729	-5.778485
Elevation (m asl)	1505	1505
Loop type	Square	Square
Loop side	30 m	60 m
Depth	45 m	90 m
Geomorphology	Peat bog	Peat bog

DD: decimal degrees; m asl: metres above sea level

Table 2. Results of interpreting Vertical Electrical Soundings. Error of fit (RMS) between the real and apparent resistivity model varies from 3.5% - 10.8%. Individually, each layer presents thickness and resistivity equivalences regarding to the proposed value. Every equivalence ratio in thickness (Kh) and resistivity (Kro) is averaged (ΣK/2) when differences are small (Kh-Kro <1), but for larger values (Kh-Kro ≥1), as for VES 6 and VES 7, equivalences are shown separately (by thickness and resistivity). The third layer (H3, Rho_3) may present significant resistivity equivalences for VES 6. In VES 8 and VES 7 layer 4 is the most equivalent regarding resistivities (Kh-Kro ratios of 10 or higher). Nevertheless, equivalence thickness also exist in VES 7.

	VES 1	VES 2	VES 3	VES 4	VES 5	VES 6	VES 7	VES 8	VES 9
Lat. (DD)	40.317341	40.317188	40.317116	40.323233	40.321486	40.319769	40.318432	40.318500	40.321286
Long. (DD)	-5.778121	-5.780374	-5.776150	-5.776939	-5.778444	-5.779021	-5.779578	-5.779758	-5.778895
Elev. (m asl)	1518	1509	1600	1498	1505	1506	1505	1505	1503
AB disposition	ENE-WSW	E - W	NNW-SSE	NNW-SSE	NNW-SSE	WNW-ESE	NW-SE	NE-SW	N-S
AB/2 (m)	56	32	100	75	133	133	133	133	75
H1 (m)	0.9	1	1	0.6	0.6	1	1	1.3	0.9
Rho_1 (Ωm)	1274	9873	27179	1755	4800	1801	1618	1921	1159
ΣK/2	1.2	1.15	2.43	1.87	1.2	1.08	1.08	1.04	1.31
H2 (m)	9.4	4.4	6	6.2	3.4	5.1	15.9	20.8	2.8
Rho_2 (Ωm)	10905	14612	28607	14322	2040	2754	4798	5221	731
ΣK/2	1.05	1.15	1.11	1.04	1.02	1.45	1.34	1.02	1.28
H3 (m)	-	-	25.5	-	20.6	4.2	13.6	75.6	9.3
Rho_3 (Ωm)	540	810	6408	2100	282	1941	2397	565	2341
ΣK/2	1.25	1.02	1.03	1.01	1.03	1.98 / 8.1	3.87/1.73	1.17	1.31
H4 (m)	-	-	-	-	-	16.8	66.5	-	27.8
Rho_4 (Ωm)	-	-	1289	-	5340	3161	409	60665	352
ΣK/2	-	-	1.04	-	1.06	1.33	1.81	10	1.81
Rho_5 (Ωm)	-	-	-	-	-	1441	36486	-	42196
K	-	-	-	-	-	1.01	10	-	10
RMS (%)	5..6	5.6	3.87	5.6	10.6	3.4	4.5	3.5	3.6
Ke (%)	2	2	1	1.2	2	0.7	0.85	2	1.8

DD: decimal degrees; m asl: metres above sea level; AB/2: the maximum electrode aperture in half the space; H, thicknesses

Table 3. Summary of results of seismic refraction P waves.

	Thickness (m)					Velocity
Profile	RS1	RS2	RS3	RS4	RS5	m/s
Mostly sub-sonic	2.0-4.0	3.0-6.0	0.0-6.5	-	0.6-4.7	<500
G1-G2 (DS 3)	8.0	7.0-10.0	10.0	5.3-6.7	-	500-700
				-	-	700-900
G2 (DS 2)	>8.0.	>10.0	-	-	3.6-6.0	1200-1500
Weathered granite			>10.0	-	>6.0	1500-1700
Granite	ND	ND	ND	>6.0	ND	>2000

ND, no detected;G1 and G2, Vertical Electrical Sounding resistivity units; DS 2 and DS 3, Depositional sequences

Highlights

- The surficial and subsurficial geology of Navamuño depression was established
- Using geophysical methods, the infill deposits have been interpreted
- The genetic implications of subsidence and ice-dammed processes have been analysed

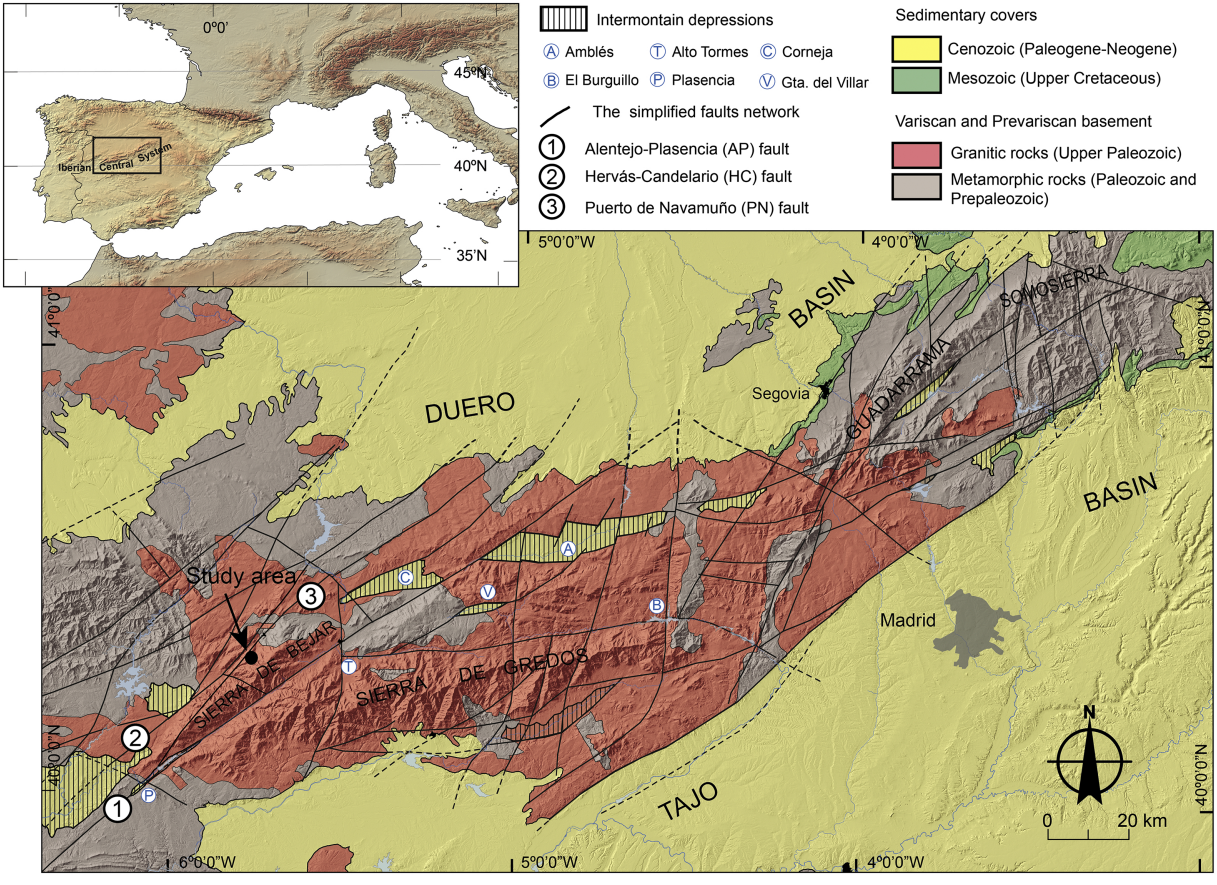
0°0'
45°N
40°N
35°N
Iberian Central System
Intermontain depressions
Ⓐ Amblés
Ⓑ El Burguillo
Ⓒ Corneja
Ⓟ Plasencia
Ⓣ Alto Tormes
Ⓥ Gta. del Villar
The simplified faults network
1 Alentejo-Plasencia (AP) fault
2 Hervás-Candelario (HC) fault
3 Puerto de Navamuño (PN) fault
Sedimentary covers
Cenozoic (Paleogene-Neogene)
Mesozoic (Upper Cretaceous)
Variscan and Prevariscan basement
Granitic rocks (Upper Paleozoic)
Metamorphic rocks (Paleozoic and Prepaleozoic)
5°0'0"W
4°0'0"W
41°0'0"N
40°0'0"N
6°0'0"W
DUERO
BASIN
SOMOSIERRA
GUADARRAMA
Segovia
Madrid
Study area
SIERRA DE BEJAR
SIERRA DE GREDOS
TAJO
N
0
20 km

Figure 1

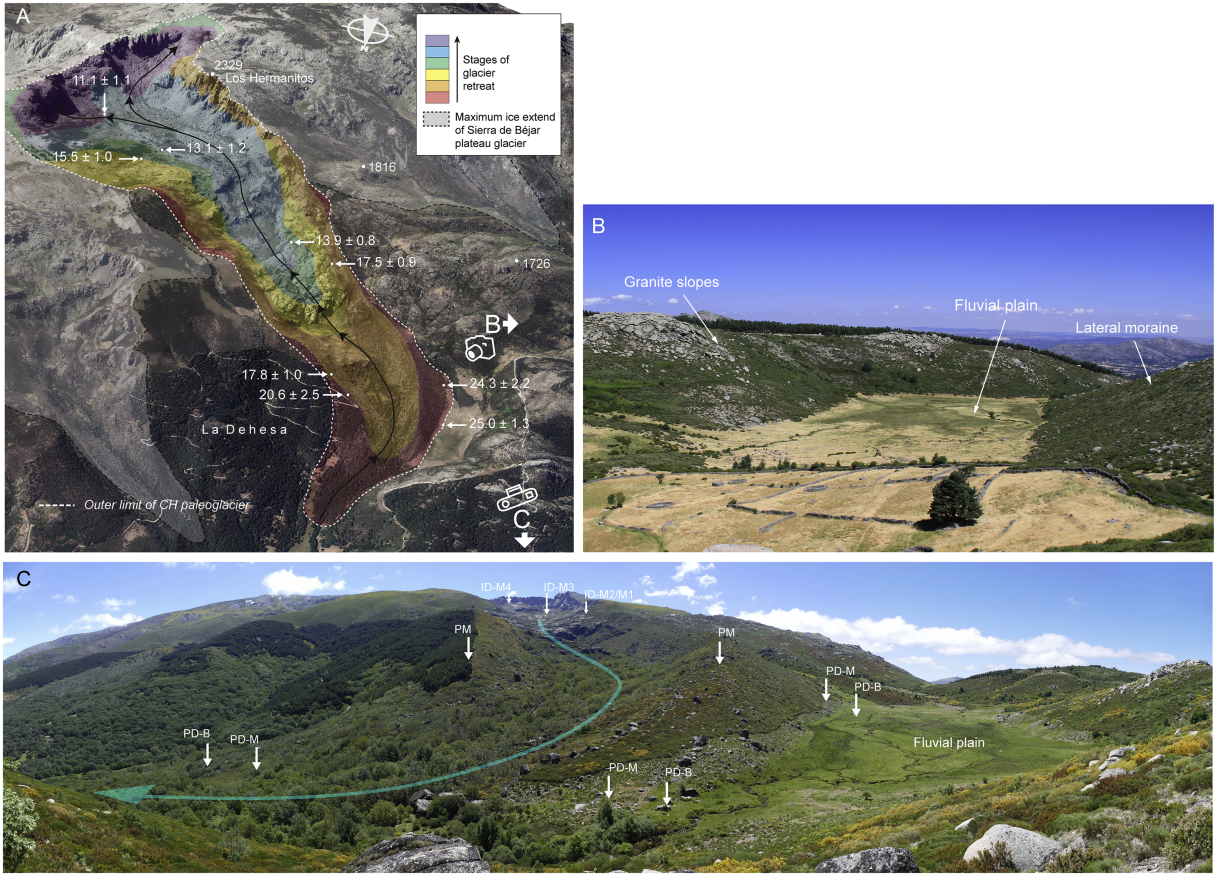
A
11.1 ± 1.1
2329
Los Hermanitos
15.5 ± 1.0
13.1 ± 1.2
1816
13.9 ± 0.8
17.5 ± 0.9
1726
B
17.8 ± 1.0
20.6 ± 2.5
24.3 ± 2.2
25.0 ± 1.3
La Dehesa
Outer limit of CH paleoglacier
C
Stages of glacier retreat
Maximum ice extend of Sierra de Béjar plateau glacier
B
Granite slopes
Fluvial plain
Lateral moraine
C
ID-M4
ID-M3
ID-M2/M1
PM
PM
PD-M
PD-B
PD-B
PD-M
Fluvial plain
PD-M
PD-B

Figure 2

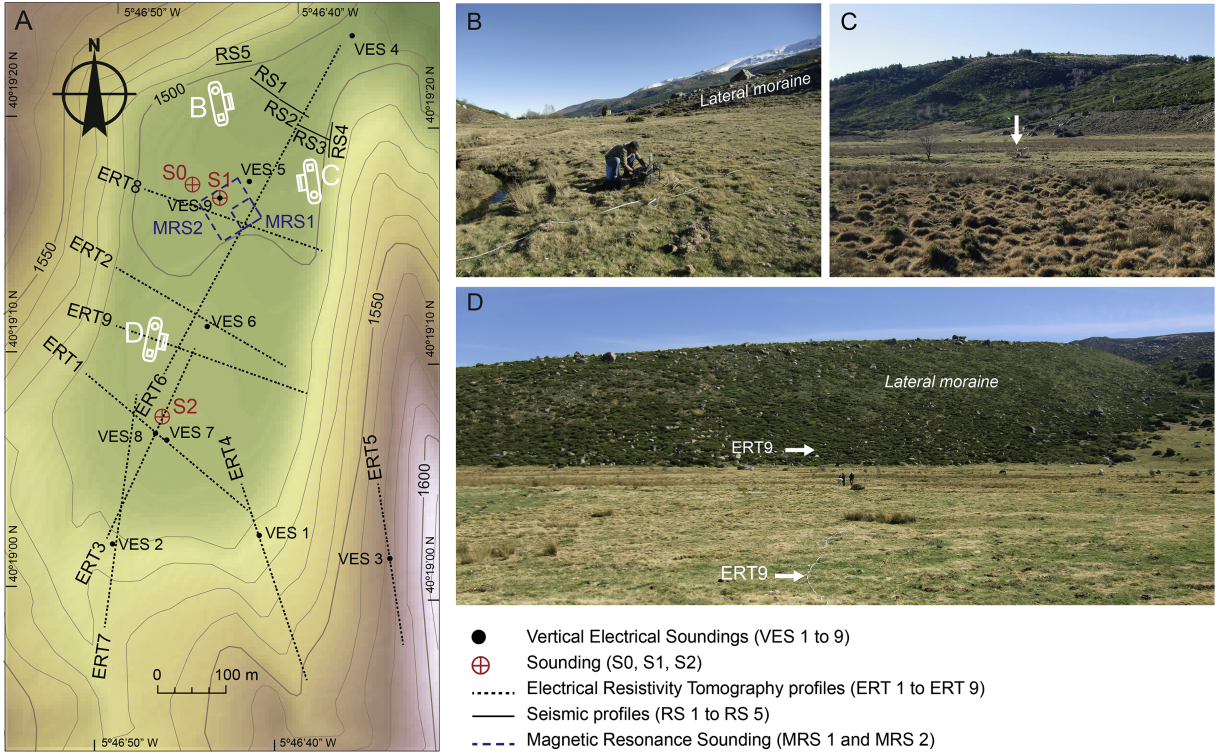
A
5°46'50" W
5°46'40" W
40°19'20 N
40°19'10 N
40°19'00 N
N
RS5
RS1
RS2
RS3
RS4
1500
B
C
VES 4
VES 5
VES 9
S0
S1
MRS2
MRS1
ERT8
ERT2
1550
ERT9
D
VES 6
ERT1
ERT6
S2
VES 8
VES 7
ERT4
ERT5
1600
VES 1
VES 2
VES 3
ERT3
ERT7
0
100 m
B
Lateral moraine
C
D
Lateral moraine
ERT9
ERT9
Vertical Electrical Soundings (VES 1 to 9)
Sounding (S0, S1, S2)
Electrical Resistivity Tomography profiles (ERT 1 to ERT 9)
Seismic profiles (RS 1 to RS 5)
Magnetic Resonance Sounding (MRS 1 and MRS 2)

Figure 3

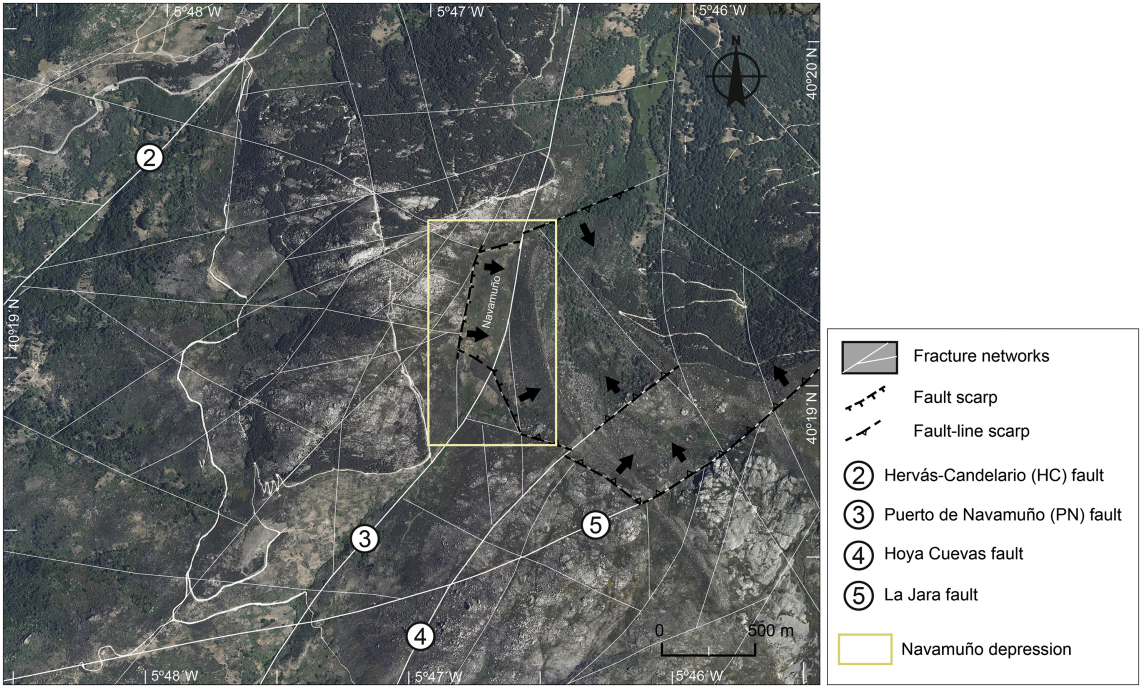
5°48 W
5°47 W
5°46 W
40°20 N
40°19 N
N
Navamuño
2
3
4
5
0
500 m
Fracture networks
Fault scarp
Fault-line scarp
2 Hervás-Candelario (HC) fault
3 Puerto de Navamuño (PN) fault
4 Hoya Cuevas fault
5 La Jara fault
Navamuño depression

Figure 4

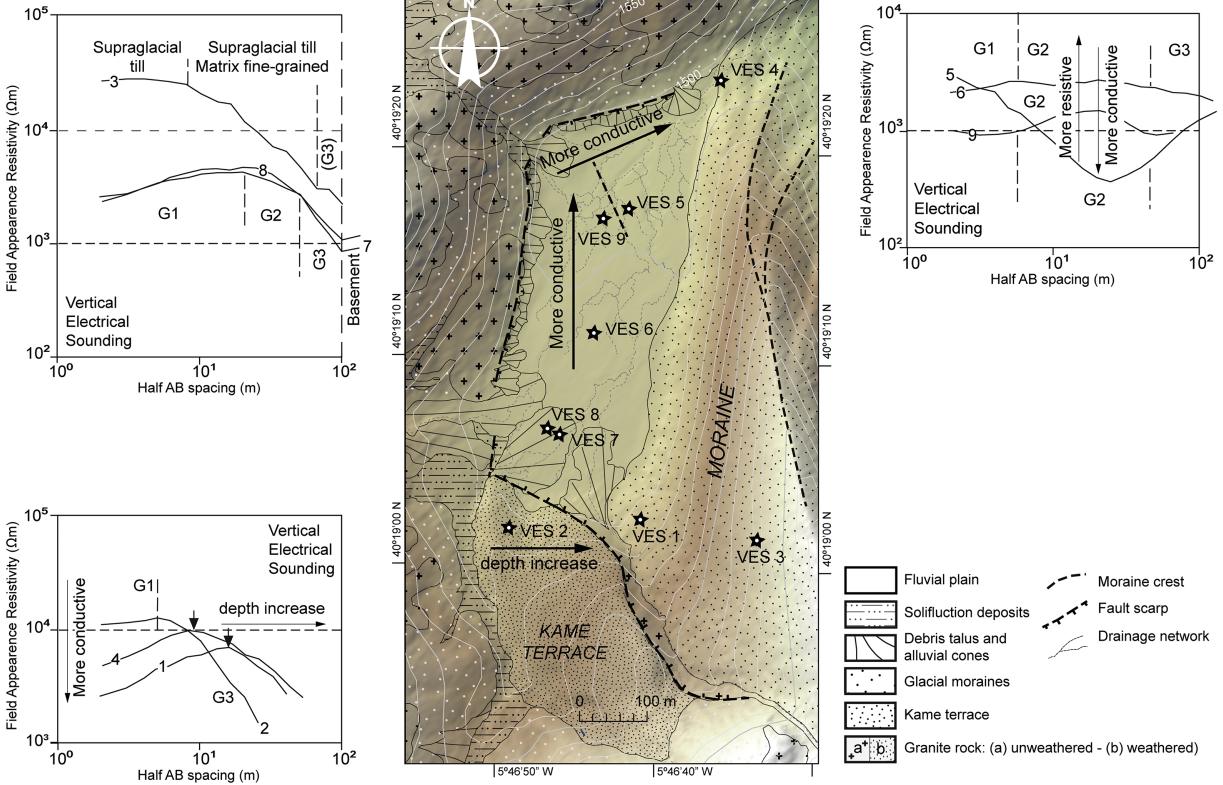
Supraglacial till
Supraglacial till
Matrix fine-grained
Field Appearence Resistivity (Ωm)
Half AB spacing (m)
Vertical Electrical Sounding
G1
G2
G3
(G3)
Basement
5°46'50" W
5°46'40" W
40°19'20 N
40°19'10 N
40°19'00 N
More conductive
VES 1
VES 2
VES 3
VES 4
VES 5
VES 6
VES 7
VES 8
VES 9
MORAINE
KAME TERRACE
depth increase
0
100 m
More resistive
Fluvial plain
Solifluction deposits
Debris talus and alluvial cones
Glacial moraines
Kame terrace
Granite rock: (a) unweathered - (b) weathered
Moraine crest
Fault scarp
Drainage network

Figure 5

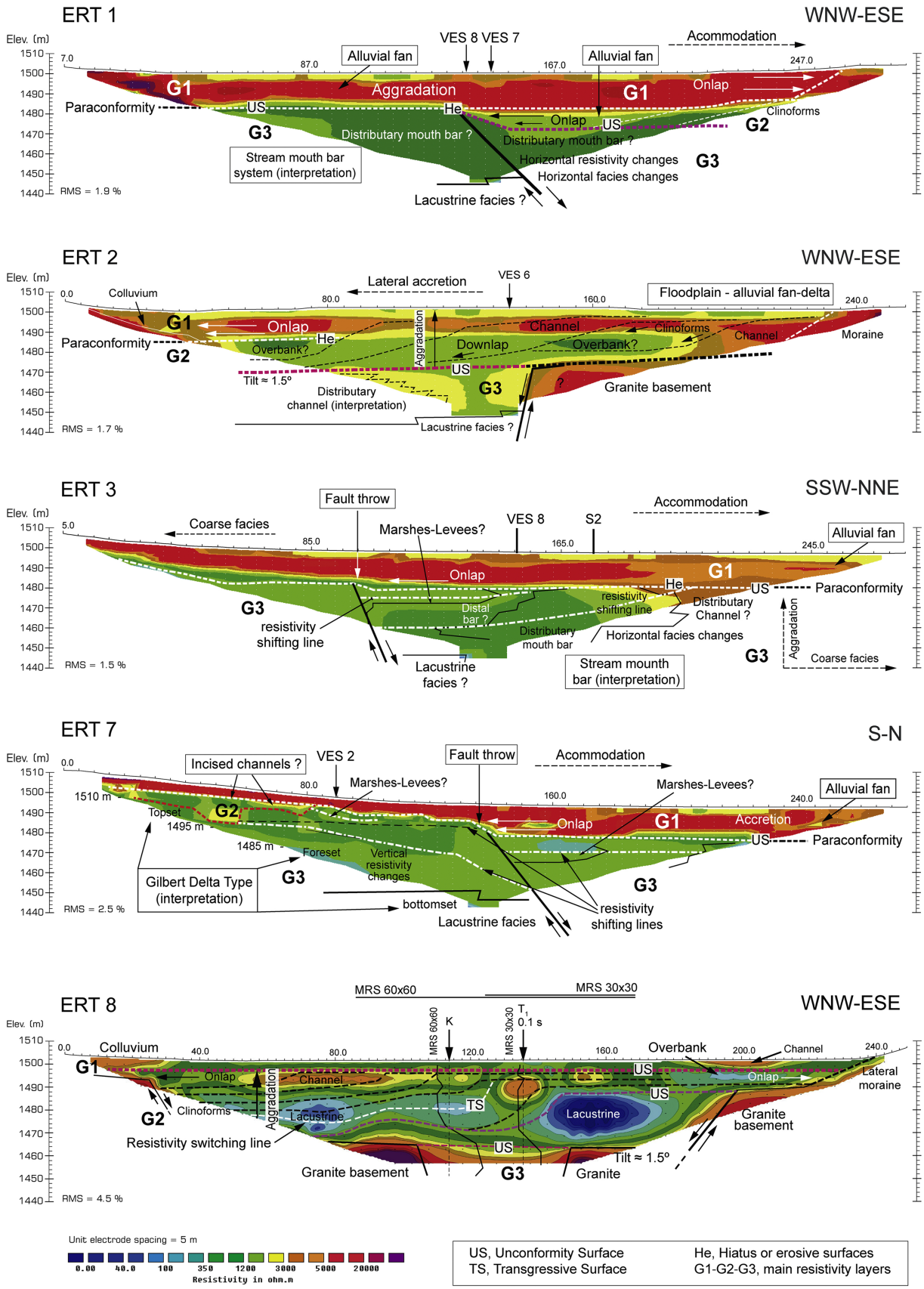
ERT 1
WNW-ESE
Elev. (m)
VES 8 VES 7
Acommodation
Alluvial fan
Alluvial fan
Aggradation
G1
G1
Onlap
Paraconformity
US
He
Onlap
US
Clinoforms
G3
G2
Distributary mouth bar ?
Distributary mouth bar ?
Stream mouth bar system (interpretation)
Horizontal resistivity changes
Horizontal facies changes
G3
Lacustrine facies ?
RMS = 1.9 %
ERT 2
WNW-ESE
Elev. (m)
Lateral accretion
VES 6
Colluvium
Floodplain - alluvial fan-delta
G1
Onlap
Aggradation
Channel
Clinoforms
Channel
Moraine
Paraconformity
He
Downlap
Overbank?
Overbank?
G2
US
Tilt ≈ 1.5°
G3
?
Granite basement
Distributary channel (interpretation)
Lacustrine facies ?
RMS = 1.7 %
ERT 3
SSW-NNE
Elev. (m)
Fault throw
Accommodation
Coarse facies
Marshes-Levees?
VES 8
S2
Alluvial fan
Onlap
G1
He
US
Paraconformity
G3
Distal bar ?
resistivity shifting line
Distributary Channel ?
resistivity shifting line
Distributary mouth bar
Horizontal facies changes
G3
Aggradation
Coarse facies
Lacustrine facies ?
Stream mounth bar (interpretation)
RMS = 1.5 %
ERT 7
S-N
Elev. (m)
Incised channels ?
VES 2
Fault throw
Acommodation
Marshes-Levees?
Marshes-Levees?
Alluvial fan
1510 m
Topset
1495 m
G2
Onlap
G1
Accretion
US
Paraconformity
1485 m
Foreset
Vertical resistivity changes
Gilbert Delta Type (interpretation)
G3
G3
bottomset
Lacustrine facies
resistivity shifting lines
RMS = 2.5 %
ERT 8
WNW-ESE
Elev. (m)
MRS 60x60
MRS 30x30
K
T1 0.1 s
Colluvium
Overbank
Channel
G1
Onlap
Aggradation
Channel
US
Onlap
Lateral moraine
G2
Clinoforms
Lacustrine
TS
US
Lacustrine
Granite basement
Resistivity switching line
US
Tilt ≈ 1.5°
Granite basement
G3
Granite
RMS = 4.5 %
Unit electrode spacing = 5 m
0.00 40.0 100 350 1200 3000 5000 20000
Resistivity in ohm.m
US, Unconformity Surface
TS, Transgressive Surface
He, Hiatus or erosive surfaces
G1-G2-G3, main resistivity layers

Figure 6

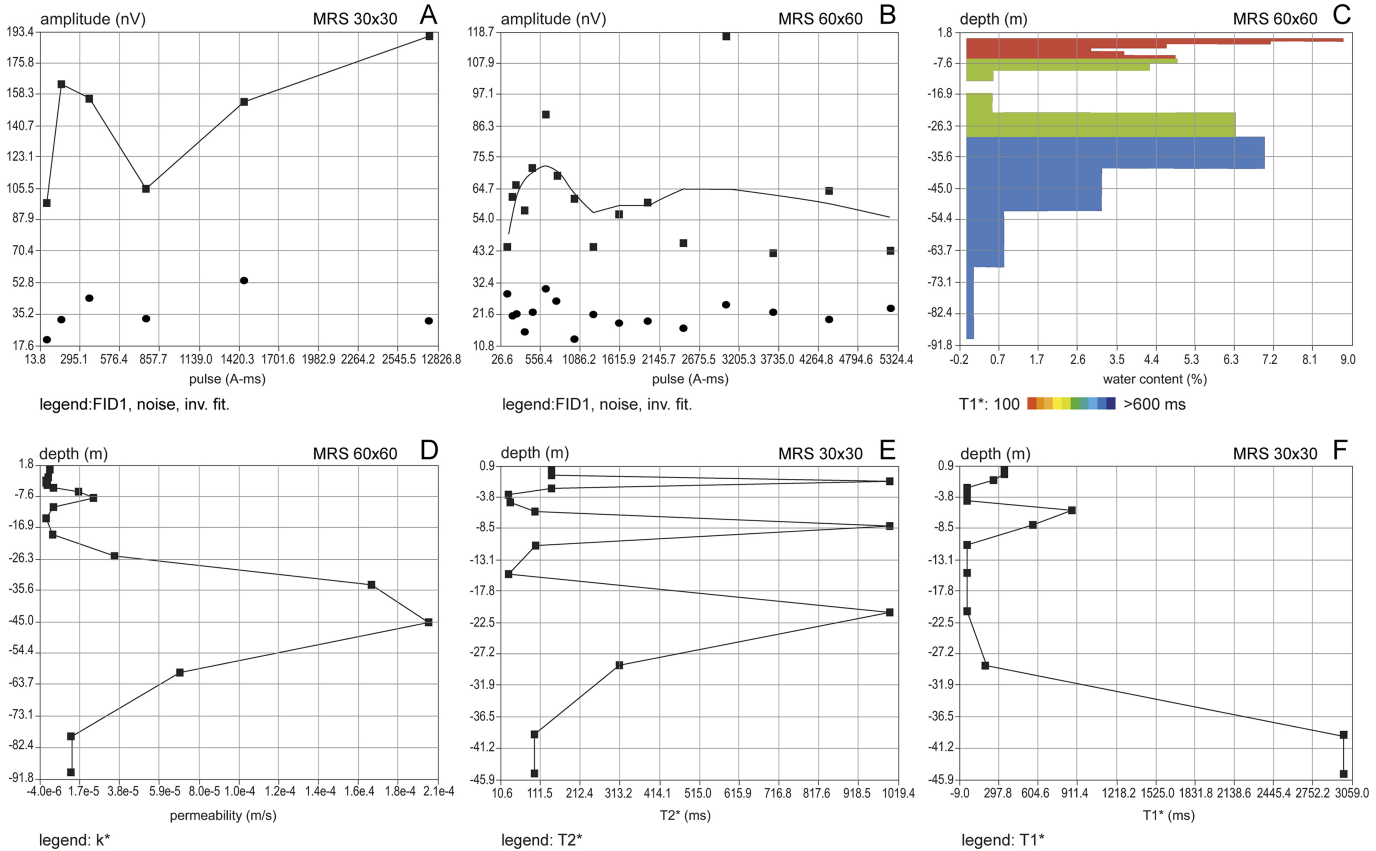
amplitude (nV)
MRS 30x30
A
193.4
175.8
158.3
140.7
123.1
105.5
87.9
70.4
52.8
35.2
17.6
13.8
295.1
576.4
857.7
1139.0
1420.3
1701.6
1982.9
2264.2
2545.5
12826.8
pulse (A-ms)
legend:FID1, noise, inv. fit.
amplitude (nV)
MRS 60x60
B
118.7
107.9
97.1
86.3
75.5
64.7
54.0
43.2
32.4
21.6
10.8
26.6
556.4
1086.2
1615.9
2145.7
2675.5
3205.3
3735.0
4264.8
4794.6
5324.4
pulse (A-ms)
legend:FID1, noise, inv. fit.
depth (m)
MRS 60x60
C
1.8
-7.6
-16.9
-26.3
-35.6
-45.0
-54.4
-63.7
-73.1
-82.4
-91.8
-0.2
0.7
1.7
2.6
3.5
4.4
5.3
6.3
7.2
8.1
9.0
water content (%)
T1*: 100
>600 ms
depth (m)
MRS 60x60
D
1.8
-7.6
-16.9
-26.3
-35.6
-45.0
-54.4
-63.7
-73.1
-82.4
-91.8
-4.0e-6
1.7e-5
3.8e-5
5.9e-5
8.0e-5
1.0e-4
1.2e-4
1.4e-4
1.6e-4
1.8e-4
2.1e-4
permeability (m/s)
legend: k*
depth (m)
MRS 30x30
E
0.9
-3.8
-8.5
-13.1
-17.8
-22.5
-27.2
-31.9
-36.5
-41.2
-45.9
10.6
111.5
212.4
313.2
414.1
515.0
615.9
716.8
817.6
918.5
1019.4
T2* (ms)
legend: T2*
depth (m)
MRS 30x30
F
0.9
-3.8
-8.5
-13.1
-17.8
-22.5
-27.2
-31.9
-36.5
-41.2
-45.9
-9.0
297.8
604.6
911.4
1218.2
1525.0
1831.8
2138.6
2445.4
2752.2
3059.0
T1* (ms)
legend: T1*

Figure 7

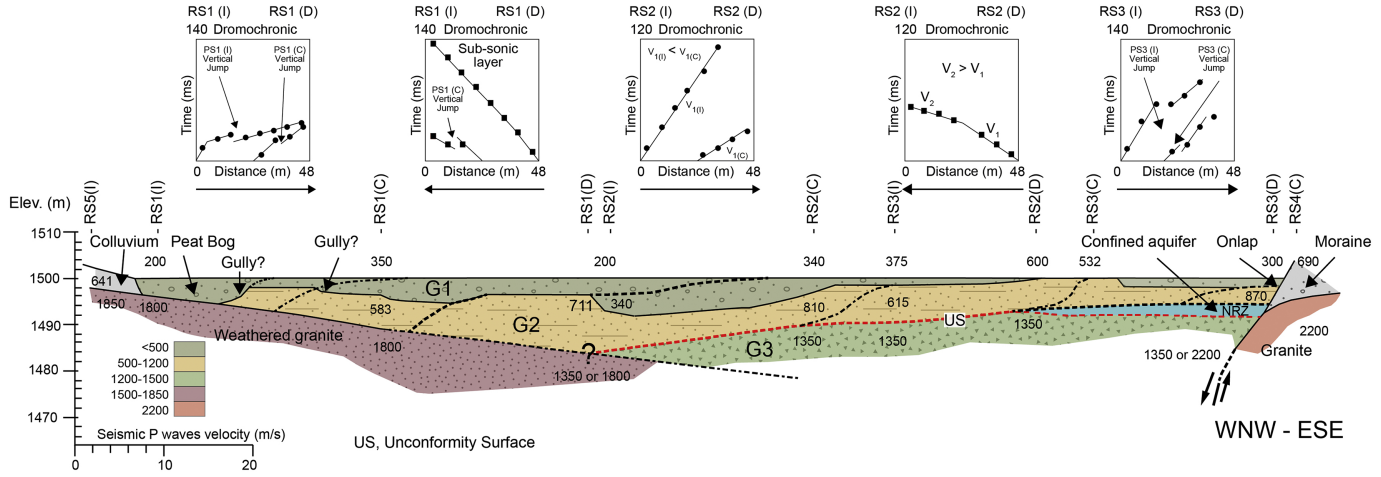
RS1 (I) RS1 (D)
140 Dromochronic
PS1 (I) Vertical Jump
PS1 (C) Vertical Jump
Time (ms)
0 Distance (m) 48
RS1 (I) RS1 (D)
140 Dromochronic
Sub-sonic layer
PS1 (C) Vertical Jump
RS2 (I) RS2 (D)
120 Dromochronic
V1(I) < V1(C)
V1(I)
V1(C)
RS2 (I) RS2 (D)
120 Dromochronic
V2 > V1
V2
V1
RS3 (I) RS3 (D)
140 Dromochronic
PS3 (I) Vertical Jump
PS3 (C) Vertical Jump
Elev. (m)
RS5(I) - RS1(I) - RS1(C) - RS1(D) - RS2(I) - RS2(C) - RS3(I) - RS2(D) - RS3(C) - RS3(D) - RS4(C)
1510
1500
1490
1480
1470
Colluvium
Peat Bog
Gully?
Gully?
200
350
200
340
375
600
532
Confined aquifer
Onlap
Moraine
300
690
641
1850
1800
583
711
340
810
615
870
G1
G2
G3
NRZ
US
2200
Granite
Weathered granite
1800
1350
1350
1350
1350 or 2200
1350 or 1800
?
<500
500-1200
1200-1500
1500-1850
2200
Seismic P waves velocity (m/s)
0
10
20
US, Unconformity Surface
WNW - ESE

Figure 8

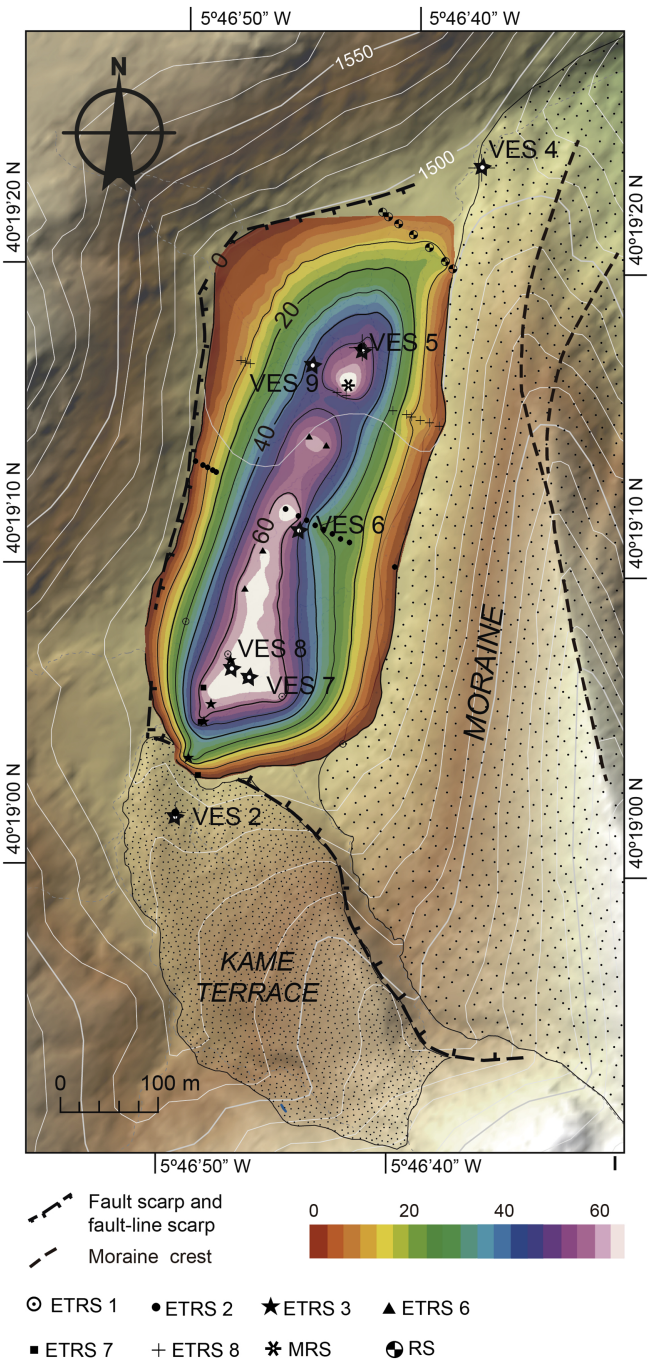
5º46'50" W
5º46'40" W
40º19'20 N
40º19'10 N
40º19'00 N
N
1550
1500
VES 4
VES 5
VES 9
VES 6
VES 8
VES 7
VES 2
0
20
40
60
MORAINE
KAME
TERRACE
0
100 m
Fault scarp and
fault-line scarp
Moraine crest
0
20
40
60
ETRS 1
ETRS 2
ETRS 3
ETRS 6
ETRS 7
ETRS 8
MRS
RS

Figure 9